Cooling paths during the Mesozoic Extensional Tectonics of NE China: example from the South Liaodong Peninsula Metamorphic Core Complex

Wei Lin, Patrick Monié, Michel Faure, Urs Schärer, Yonghong Shi, Nicole Le Breton, Qingchen Wang

To cite this version:

Wei Lin, Patrick Monié, Michel Faure, Urs Schärer, Yonghong Shi, et al.. Cooling paths during the Mesozoic Extensional Tectonics of NE China: example from the South Liaodong Peninsula Metamorphic Core Complex. Journal of Asian Earth Sciences, 2011, 42 (5), pp.1048-1065. 10.1016/j.jseaes.2010.09.007 . insu-00528171

HAL Id: insu-00528171
https://insu.hal.science/insu-00528171

Submitted on 25 Oct 2010

Cooling paths during the Mesozoic Extensional Tectonics of NE China: example from the South Liaodong Peninsula Metamorphic Core Complex

Wei Lin[a, *], Patrick Monié[b], Michel Faure[c], Urs Schärer[d], Yonghong Shi[e], Nicole Le Breton[c], Qingchen Wang[a]

[a] *State Key Laboratory of Lithospheric Evolution, Institute of Geology and Geophysics, Chinese Academy of Sciences, Beijing 100029, China*

[b] *Géosciences Montpellier, UMR-CNRS 5243, Université Montpellier 2, Pl. E.-Bataillon, F-34095 Montpellier Cedex, France*

[c] *Institut des Sciences de la Terre d'Orléans, UMR-CNRS 6113, Bâtiment Géosciences, Université d'Orléans, F-45067 Orléans Cedex 2, France*

[d] *University of Nice-Sophia Antipolis, CNRS-UMR 6526, parc Valrose, F-06108 Nice,*

France

[e] *Department of Geology, School of Resource and Environment Engineering, Hefei University of Technology, Tunxi Road 193, Hefei, Anhui Province 230009, China*

*Corresponding author: W. Lin

Tel.:+86 10 82998546; fax: +86 10 62010846. E-mail address: linwei@mail.iggcas.ac.cn

Abstract

The South Liaodong Peninsula massif is the easternmost Mesozoic Metamorphic Core Complex, recognized in Eastern China. It provides a good example of the combination of ductile shearing, synkinematic plutonism and polyphase exhumation. The Jurassic granodioritic plutons, located at the footwall of the detachment normal fault, and dated here at ca 160 Ma, recorded two different phases of cooling. A slow cooling regime of about 3-10°C/my prevailing before 122 Ma, was followed by a significant increase in cooling rate of about 40-55°C/my after that time. By contrast, a single fast cooling path was recorded by the Cretaceous monzogranite situated in the footwall of the detachment normal fault. This result indicates that the Jurassic and Cretaceous plutons recorded different exhumation processes: a Jurassic slow or negligible exhumation and a Cretaceous fast one assisted by normal faulting. These two cooling stages correspond to distinct geodynamic processes during the Jurassic and Cretaceous. Extensional tectonics seems not significant before Early Cretaceous. The second stage, dominated by an extensional regime which develops after ca 120 Ma, is tentatively correlated to the lithosphere removal of the North China Craton.

Key words: Metamorphic Core Complex; Two cooling stage; Radiometric ages; Lithospheric removal; North China Craton

1. **Introduction**

The eastern part of north China represents an important tectonic element of the North China Craton (NCC). It is composed of several Archean blocks assembled during Early Paleoproterozoic times (Kusky and Li 2003; Zhao et al. 2005; Faure et al. 2007; Trap et al. 2007) and covered by Meso and Neoproterozoic sediments (SBGMR, 1989; HBGMR, 1989). During the Late Paleozoic to Early Mesozoic, the tectonic evolution of the NCC was essentially located along its margins (Yin and Nie, 1993, 1996; Zhai et al., 2004). Along its southern border, the Qinling-Dabie-Sulu orogenic belt (Fig. 1A) corresponds to the collision zone between the NCC and the South China Block (SCB). As indicated by structural and metamorphic studies of UHP rocks, the lithosphere convergence accommodated more than 200 km of north-directed continental subduction (Mattauer et al., 1985; Faure et al., 2003a, b; Hacker et al., 1998, 2006 and reference therein; Fig. 1A). To the north, the Central Asian Orogenic Belt (CAOB, Fig. 1A) corresponds to the collision zone between the NCC and the Paleozoic Mongolian arcs, attached during late Permian to Early Triassic times (Wang and Liu, 1986; Lamb and Badarch, 1997; Sengor and Natal'in, 1996; Xiao et al., 2003; Shang, 2004; Lin et al., 2008a).

Recently, the geology of the NCC has attracted great attention because of the coexistence of Ordovician diamondiferous kimberlites, Mesozoic lamprophyre-basalt and Cenozoic basalts in this craton, especially in the western part of Shandong province and in the South of Liaodong Peninsula. Silicate inclusions in diamonds, peridotites and disaggregated minerals in Ordovician kimberlites indicate the presence of a thick (~200 km), cold and refractory lithospheric keel beneath the NCC prior to the Paleozoic (Griffin et al., 1998; Xu, 2001). Based on geophysical data and petrological studies of mantle xenoliths from Late Mesozoic to Early Cenozoic basalts, it has been argued that the present lithosphere thickness lies between 120 km and 70 km (Fan and Menzies, 1992; Menzies et al., 1993; Menzies and Xu, 1998; Griffin et al., 1998; Zhang and Zheng, 2003; Deng et al., 2004; Zhang, 2005). This means that, during Late Mesozoic, the lithosphere lost more than 80 km. At crustal level, lithospheric thinning is accommodated by ductile and brittle normal faulting. This Late Mesozoic phase of extension occurred coevally with volumetrically important Jurassic-Cretaceous magmatism extending more than 4000 km, from the Okhotsk Sea in the North to Vietnam in the South (Zorin, 1999; Ren et al., 2002; Meng, 2003; Wu et al., 2005a). In East China, rift basins and related metamorphic complexes were recognized very early, even before the development of plate tectonics (Huang, 1945). Several models have been proposed to interpret the Mesozoic evolution of the NCC, involving processes such as rifting (Tian et al., 1992), mantle plume (Deng et al., 1998, 2004), thermal and chemical erosion of the lithospheric mantle (Xu, 1999, 2001), basaltic underplating (Zhang and Sun, 2002), mantle delamination (Gao et al., 1998, 2002) and subduction induced rollback (Ren et al., 2002). Both the exact timing and the processes of NCC thinning remain disputed. In NE China, the South Liaodong peninsula has been recognized as a Cretaceous metamorphic core complex (MCC) with abundant plutonic rocks (e.g. Yin and Nie, 1993; Liu et al., 2005; Lin et al., 2008b and enclosed references). Therefore, we have undertaken $^{40}Ar/^{39}Ar$ and U/Pb geochronological studies from the granitoids of this area, using a suite of minerals with different closure temperatures, in order to derive the cooling path experienced by this MCC.

2. Geological framework of south Liaodong peninsula massif

In the Liaoning Province of NE China, the south Liaodong peninsula massif (Fig. 1) is composed of metamorphic and magmatic rocks, with Archean and Paleoproterozoic rocks occuping about half of the complex (Yin and Nie, 1996; Lu et al., 2004; Faure et al., 2004;

Li et al., 2005). Neoproterozoic and Paleozoic sediments overlie metamorphic rocks, which are intruded by Mesozoic granitoids (Wu et al., 2005a, b; Yang et al., 2007a, b and c). Mesozoic to Cenozoic terrigeneous rocks occur in fault-bounded troughs, suggesting basin formation related to extension (Allen et al., 1997; Okada, 1999; Ren et al., 2002). Structurally, the south Liaodong peninsula massif is a Cretaceous asymmetric metamorphic core complex (MCC) with a NE-SW trending long axis (Fig. 1; Liu et al., 2005; Yang et al., 2007b; Lin et al., 2008b and therein references). It consists of three litho-tectonic units namely: (1) a gneissic migmatite unit, (2) a Paleo- to Mesoproterozoic micaschist and slate unit, and (3) a Neoproterozoic to Mesozoic sedimentary cover.

The south Liaodong peninsula MCC shows NW-SE trending extension direction (Liu et al., 2005; Yang et al., 2007b; Lin et al., 2008b). The Paleo-proterozoic gneisses and foliated migmatite that form the core of the MCC are heterogeneously deformed with a relatively weakly foliated core and a mylonitic shear zone at the margin. The dome boundary is a ductile detachment normal fault (Fig. 2). Two types of granitoid plutons intrude the metamorphic series. Jurassic granodiorites are pervasively foliated, whereas Early Cretaceous syntectonic monzogranitic plutons are weakly foliated except where they are involved in the detachment fault. In this latter structure the granitic rocks were converted to mylonite or ultramylonite. Kinematic shear criteria show a top-to-the-NW sense of movement along the detachment fault. As observed in the metamorphic core complexes of North America (e.g. Lister & Davis, 1989), the detachment fault of south Liaodong peninsula MCC is arched, due to syn-extensional folding around a NE-SW axis (Fig. 1). As a result, the SE dome limb appears as a top-to-the-NW thrust, which is in reality a folded normal fault. In the hanging wall of the detachment fault, the Neoproterozoic and Paleozoic sedimentary rocks are deformed by northwestward verging folds (Fig. 1; Lin et al., 2008b).

Along the ductile detachment normal fault, several samples were collected in order to constrain the time of exhumation of the south Liaodong peninsula MCC using the laser probe single grain step-heating ^{40}Ar/^{39}Ar method on biotite and amphibole and the U/Pb method on titanite fraction. Combined with the previews geochronological work (Yin & Nie, 1996; Wu et al., 2005a, 2005b; Yang et al., 2004, 2007b), we can establish the cooling history of south Liaodong peninsula MCC.

3. Geochronology

3.1. Previous Geochronological data

In the south Liaodong peninsula MCC, several previous studies provide different time constraints. Mylonitic migmatite and deformed mafic dyke yield ^{40}Ar/^{39}Ar ages between 113-110 Ma and 125-105 Ma interpreted as the age of exhumation and cooling respectively (Yin and Nie, 1996; Yang et al., 2004, 2007b). U-Pb, LA-ICP-MS dating of zircon for the medium to fine-grained monzogranites and biotite-granites gives ages in the range 135-110 Ma (Fig. 3; Wu et al., 2005a). Meanwhile, rarely exposed, 150-180 Ma old, biotite-hornblende granodiorites and tonalites were also dated or found in the study area (Wu et al., 2005b).

3.2. ^{40}Ar/^{39}Ar dating

A total of 9 mineral samples have been dated with the laser probe ^{40}Ar/^{39}Ar method using a single grain step-heating procedure. Samples were taken on both northern and southern sides of the dome in order to place age constraints on the top to the NW shearing.

The dated rocks are gneissic and mylonitic migmatites (LN66, LN85 and LN93), deformed amphibolites (LN59, LN70), orthogneiss (LN56, LN71), a mylonitized granodiorite (LN83) within the detachment zone, and an undeformed biotite granite (LN110) from the dome core (Fig. 3). Table 1 summarizes the location, lithology, dated minerals, state of deformation and ^{40}Ar/^{39}Ar results for each sample.

Dating was performed on 0.5-1 mm sized minerals separated under the binocular after coarse rock crushing. These minerals were packed in aluminium foils for fast neutron irradiation during 60 hours in the McMaster nuclear reactor together with several MMHb1 hornblende flux monitors (520.4 ± 1.7 Ma; Samson and Alexander, 1987). After irradiation, the minerals were placed on Cu-holder inside an UHV extraction system and baked for 48 hours at 200°C. Step-heating experiments were conducted on single grains with the laser operating in the continuous mode, by increasing its power at each step. There was no direct control of the temperature applied to the samples. Only their infrared colour change was checked with a camera placed above the sample chamber. The analytical device consists of: (a) a multiline continuous 6 W argon-ion Lexel 3500 laser; (b) a beam shutter for selection of exposure times, typically 30 s for individual steps; (c) divergent and convergent lenses for definition of the beam diameter; (d) a small inlet line for the extraction and purification of gases; (e) a MAP 215-50 noble gas mass spectrometer. Each analysis involves 5 min for gas extraction and cleaning and 15 min for data acquisition by peak switching from mass 40 to mass 36. System blanks were evaluated every three analyses and ranged from 3.10^{-12} cc for ^{40}Ar to 4.10^{-14} cc for ^{36}Ar. Ages and errors were calculated according to McDougall and Harrison (1999). Complete results are reported in Table 1 and illustrated as age spectra. The quoted errors represent one sigma deviation and include uncertainty on the monitor age and its ^{40}Ar/^{39}Ar ratio. This uncertainty is considered in the calculation of the plateau and total age errors. Data have been also reported in ^{36}Ar/^{40}Ar vs. ^{39}Ar/^{40}Ar correlation plots and Table 2 compares the results given by the two graphical approaches.

Age spectra of five biotites are reported on figure 4 (a-e). These spectra are flat for a large percentage of the argon released. Most of them do not satisfy the strict definition of a plateau age in the sense of Fleck et al. (1977), i.e., 3 or more contiguous heating steps comprising 50% or more of the ^{39}Ar released and overlapping at the two sigma confidence level. This is partly due to the fact that the laser probe degassing of single grain provides more details about distribution of argon isotopes within the mineral lattice than the bulk sample step-heating technique that only gives a global view of this distribution. Therefore, and more frequently for biotites, age spectra display small internal age variations that probably result from degassing of different textural and chemical microdomains. For the least discordant portion of these spectra, we calculate pseudo-plateau ages that are statistically similar to the intercept ages obtained in the ^{36}Ar/^{40}Ar vs. ^{39}Ar/^{40}Ar correlation plot (Table 1) with initial ^{36}Ar/^{40}Ar ratios that do not significantly deviate from the present day atmospheric value (1/295.5). These pseudo-plateau ages range from 116.9 ± 1.4 Ma to 124.1 ± 1.3 Ma and the corresponding intercept ages between 118.1 ± 1.3 Ma to 124.9 ± 1.2 Ma (one sigma error). Cooling ages from mylonitized rocks do not reveal significant age differences between the southern and northern limbs of the dome and they agree with the biotite cooling age of an undeformed granite inside the dome also (sample LN110).

Four amphibole age spectra are reported in figure 4 (f-i), together with Ca/K spectra. Two types of profile can be observed, depending on the nature of the protolith. For mylonitic granodiorite (LN83) and gneissic migmatites (LN85), the age spectra are relatively flat yielding pseudo-plateau ages respectively of 121.7 ± 1.6 and 116.4 ± 1.5 Ma, being in agreement with the biotite dates. In the ^{36}Ar/^{40}Ar vs. ^{39}Ar/^{40}Ar correlation plot, sample LN85 has an intercept age similar to the pseudo-plateau. By contrast, sample LN83 has an intercept age that is by 4 Ma younger than its pseudo-plateau age, and its initial argon ratio above 295.5 suggests the presence of a minor amount of excess argon. The age spectra from two amphibolites (Fig. 4 f and g) are strongly discordant and characterized by a bump in the middle portion of the spectrum; no correlation with Ca/K variations can be observed. During step heating, apparent ages increase from minimum values in the range 100-130 Ma to maxima of 255 Ma for LN 59 and 331 Ma for LN 70. Then, ages decrease to values that range from 150 to 280 Ma. No intercept age can be defined for these two amphiboles.

3.3. U-Pb dating

A granodioritic intrusion (LN 82) occurring close to the detachment zone in the western side of the massif was collected to date primary magmatic titanite that crystallized from the granitic melt. The euhedral grains vary in size from a few micro-meters to about 0.4 mm, with a mean length of about 0.2 mm. In pleochroism, the transparent grains range from honey-brown to yellow carrying in some cases opaque inclusions, typical of titanites from rocks formed by crustal melting (Schärer and Labrousse, 2003). After mechanical abrasion with pyrite (Krogh, 1982), the 4N HNO_3-washed titanites were individually selected to constitute size-fractions representative of the entire population. Seven such fractions were analyzed for U-Pb (Table 3), as well as cogenetic K-feldspar to determine initial Pb isotopic composition at the time of melt crystallization. The 0.22-0.34 mg fractions carry between 119 and 141 ppm of U, and corresponding radiogenic Pb lies between 3.17 and 3.69 ppm. In the Concordia plot, (Fig. 5) six of the analyses yield ages that are identical within analytical uncertainty (ellipses), lying slightly to the left of the

Concordia curve. One fraction yields younger ages. Although the deviation of five fractions from the curve lies on the order of only 1%, it is analytically significant, whereas two analyses lie on the curve, with one having identical ages to the other grain fractions. To explain such a deviation, the following three possibilities have to be considered: (1) isotopic compositions of common Pb in K-feldspar are varying, being identical to Pb initial compositions only in some of the titanites (the concordant data), (2) the grains are affected by minor relative U-loss, and (3) deviation is due to initial disequilibrium, relative to initial excess of ^{230}Th in the ^{238}U decay chain (Schärer, 1984). To examine hypothesis (1), we have calculated the ages with model Pb isotopic compositions for upper (Zartman and Doe, 1981) and average (Stacey and Kramers, 1975) Phanerozoic and Precambrian continental crust but none of the compositions brings the individual dates on the Concordia curve. Hypothesis (2) cannot completely be ruled out; however, it is not very likely since re-opening of the U-Pb clock would result in a spread of data along their^{207}Pb/^{206}Pb slope; there is very little chance to have identical ages on 6 of 7 analyses and in particular, if one considers that both abraded and not abraded grains define the identical ages. Point (3), (excess ^{206}Pb from initial excess in ^{230}Th) is not likely because Th/U in this mineral is not high enough to cause measurable disequilibrium after more than 150 m.y. of radioactive decay (calculated from radiogenic ^{208}Pb, Table 3). However, if very recent slight titanite overgrowth has occurred it could potentially induce disequilibrium on the order of 1 percent. Presently, we cannot unambiguously ascribe the slight deviation to any of these possibilities.

Since the dominant uncertainty lies on ^{207}Pb, which is very sensitive to any change in initial Pb compositions, the mean value of ^{206}Pb/^{238}U ratios (6 fractions with identical ages) was chosen to derive the age of 160.4 ± 1.4 (2 sigma) Ma for titanite crystallization in the granodiorite. If alternatively, both ^{206}Pb/^{238}U and ^{207}Pb/^{235}U are used for calculation (including the entire extent of potential perturbation) a mean age of 154.4 ± 5.4 Ma is obtained, being within analytical error identical with the $^{206}Pb/^{238}U$ mean age.

3.4. Age interpretations

In spite of the unexplained slight deviation of about 1% from the Concordia curve, the U-Pb ages unambiguously document granodiorite emplacement around 160 Ma, i.e. in Middle Jurassic times (Dogger). Since the U-Pb chronometer behaves as a closed system above 630° C (Zhang and Schärer, 1996) this age can be considered to reflect the time of crystallization of the granodioritic magma within the rather cool country gneisses. In the study area, Middle Jurassic ages are also found for three granodioritic plutons that crop out immediately near the one dated here (Wu et al., 2005b; Fig. 3). On the other hand, monzogranitic plutons intruding the south Liaodong peninsula MCC yield U/Pb Early Cretaceous ages ranging from 130 to 120 Ma (Wu et al., 2005a; Fig. 3). The tectonic setting of this magmatism will be discussed in the next section.

Concerning the subsequent tectono-metamorphic evolution, which also deformed the Jurassic granites, $^{40}Ar/^{39}Ar$ dating of amphibole and biotite gives ages of 124-110 Ma that, according to available geochronological data, are coeval with the emplacement of a second generation of early to mid-Cretaceous granitoids. Given the difference in closure temperature for the dated minerals (≈ 300° C for biotite and ≈ 550° C for amphibole, Harrison et al., 1985; Dahl, 1996), the concordance of $^{40}Ar/^{39}Ar$ ages indicates relatively fast cooling of mylonitized gneisses and granodiorites from the detachment zone, as well as the undeformed granites below. In this context, it is suggested that fast cooling was triggered by partial removal of the hanging-wall rocks during extensional tectonics, promoting fast ascent of isotherms to upper crustal levels. Structures observed in the Cretaceous monzogranitic pluton of footwall are compatible with the idea that the NW-directed movements was coeval with the generation of deep crustal melts that migrated to upper levels as denudation was progressing (Lin et al., 2008b).

Two amphiboles from the south Liaodong peninsula MCC yield strongly different age spectra having total gas ages around 200 and 280 Ma, respectively (samples LN 59 and LN 70; Fig. 4 f, g). Since the dated rocks are amphibolite boudins within Archean gneisses, it is very likely that inherited argon causes the observed age scatter. Such in excess Ar has probably not totally been released from the boudins during Cretaceous heating of Archean basement, due to the fact that these boudins were less affected by deformation and recrystallization than their host gneiss. Several biotites also display evidence for a minor contamination by excess argon, released during the first heating increments. It is very likely that such excess in biotite was trapped on the grain surface and along its lattice defects, in relation to late fluid circulation and weathering.

4. Metamorphism and microstructure of the granodiorite involved into syn-exhumational metamorphism

In the south Liaodong peninsula MCC, the Jurassic granodioritic plutons were involved into the ductile detachment fault, and experienced metamorphism and deformation during their exhumation. Petrological analysis will allow us to understand the metamorphism and deformation history of this orthogneiss. Combined with $^{40}Ar/^{39}Ar$ and U/Pb geochronological results (cf. section 3), the P-T-t path of the South Liaodong peninsula MCC can be established.

Sample LN 84 is a foliated Jurassic granodiorite (located in Fig. 1), which contains quartz, plagioclase and biotite as major phases, and garnet, calcic-amphibole (hastingsite), epidote, allanite, albite, chlorite, pyrite and titanite as secondary ones. Anhedral garnet with no inclusion was surrounded by oligoclase (Fig. 6A-D). This texture shows that oligoclase crystallized in a relatively late stage. Clastic amphibole with euhedral or subhedral habitus is oriented along the shear bands and presents an asymmetric shape consistent with the regional kinematic pattern. Chlorite distributed around amphibole indicates that it developed under retrogressive greenschist facies conditions during the late stage of deformation.

Quantitative analyses and X-ray mapping were carried out using JEOL JXA-8800R electron-probe microanalyzer (EPMA) with WDS (Wave-dispersive-spectrometry) and EDS (Energy-dispersive-spectrometry) systems at the Petrological Laboratory of Nagoya University. Accelerating voltage, specimen current and beam diameter for quantitative analyses were 15 kV, 12 nA on the Faraday cup and 2-3 μm, respectively. Well-characterized natural and synthetic phases were used as standards. The ZAF was employed for matrix correction. Amphibole nomenclature follows Leake et al. (1997) and Fe^{3+}/Fe^{2+} values were calculated with total cations number of 13, excluding Ca, Ba, Na and K (O = 23). For garnet, all iron was assumed to be ferrous and its end-member proportion (X_i) was calculated as i/(Fe + Mn + Mg + Ca).

4.1 Garnet

Garnet belongs to Mg-poor (less than 1 wt% MgO) and Mn and Ca-rich (up to12 wt% CaO) almandine-spessartite series (Fig. 6F and Table 4). X-ray mapping and quantitative analysis results show the garnet is almost homogeneous (Fig. 6E). X (mole fraction) in garnet are 0.32-0.37 of X_{Fe} [=Fe^{2+}/(Ca+Mg+Fe^{2+}+Mn)], 0.33-0.36 of X_{Ca} [=Ca/(Ca+Mg+Fe^{2+}+Mn)], 0.26-0.29 of X_{Mn} [=Mn/(Mn+Mg+Fe^{2+}+Mn)] and 0.03-0.04 of X_{Mg} [=Mg/(Ca+Mg+Fe^{2+}+Mn)] respectively (Fig. 6F and Table 4).

4.2. Amphibole

Amphiboles form several millimeter sized grains, and most of them are hastingsite with Si = 6.16-6.42 per formula unit (pfu), $^{[B]}$Na = 0.03-0.20 pfu and $^{[A]}$(Na + K) = 0.33-0.86 pfu (Fig. 7A and Table 4). TiO_2 and K_2O contents are less than 1.1 wt% and 1.9 wt%, respectively (Table 4). Due to late metamorphic re-equilibrium, hastingsite develops a retrogressive zonation with an Al^{3+} pfu decrease from 2.29 to 1.94 from core to rim. This could be indicative of a pressure decrease as shown on figure 7B.

4.3. Other minerals

Most of analyzed plagioclase consists of 65-75 % albite, 22-30 % anorthite and 0.9-5 % K-feldspar (Fig. 7C and Table 4). X_{Fe} [= Fe^{3+}/ (Fe^{3+}+Al+Cr) as total Fe as Fe^{3+}] of epidote is around 0.30; FeO and MgO for biotite are 16.94 to 18.66 wt % and 10.26 to 11.85 wt %. These minerals have no clear zoning structure in the grain of the matrix (Table 4).

5. Discussion

5.1. P-T emplacement conditions of the Jurassic granodiorite

South of Pulandian city, a mylonitized garnet bearing granodiorite yields a titanite U/Pb age of 160.4±1.4 Ma (cf. above section 3), while clastic magmatic amphibole has a $^{40}Ar/^{39}Ar$ age of 121.7±1.6 Ma. According to the isotopic closure temperature of these minerals, we can infer that the former date represents the crystallization age of the magmatic protolith and the later one corresponds to its cooling at 550 °C. Because this age is concordant with synkinematic biotite cooling ages, it is likely that ca.120 Ma ages also date the mylonitic event responsible for the final exhumation of the granodiorite.

Allanite is an important accessory mineral in granitic rocks, but less investigated in the metamorphic ones. In our sample (LN84) allanite is abundant. It shows a relatively large compositional range and a complex zonal structure as revealed by X-ray mapping (Fig. 7 D, E, F). The zonation of the epidote minerals argues for two quite different stages of crystallization. The Fe rich and Al, Ca poor rhythmic clitellums of the core developed during the magmatic stage (Jiang et al., 2003). It is more difficult to decide if the rim part of epidote crystallized during the magmatic or metamorphism stage (Hermann, 2002). According to our knowledge of the regional geology, it is likely that the epidote rim formed during the epidote-amphibolite to greenschist facies solid state metamorphism that overprinted the magmatic assemblage.

In order to ensure more accurately the peak P-T estimates for garnet-bearing gneisses, Grt-Amp-Pl (Kohn and Spear, 1990), Grt-Bt-Pl-Qtz (Wu et al., 2004), amphibole aluminum geobarometer (Hammarstrom and Zen, 1986; Holluster et al., 1987; Johnson, 1989, Schmidt, 1992), Grt-Amp (Krogh-Ravna, 2000), and Grt-Bt (Holdaway, 2000) thermometers were used. Mineral compositions of garnet core, amphibole, biotite and plagioclase have been used as they have not been disturbed by the later metamorphism as shown by the above study of composition profiles (Figs. 6E, 7A, 7B). 16 mineral pairs were selected to derive the estimates of peak P-T conditions that are listed in Table 5.

P-T estimates using the Kohn and Spear (1990) barometer and Krogh-Ravna (2000) thermometer (first two columns in Table 5) are 0.95-1.09 GPa ($\bar{x}$=1.01, 1σ=0.04 GPa) and 585-696 °C ($\bar{x}$=651°C, 1σ=31 °C). That using Wu et al. (2004) and Holdaway (2000) thermometers are 0.81-097 GPa ($\bar{x}$=0.87, 1σ=0.04GPa) and 556-582 °C ($\bar{x}$=569 °C, 1σ=8 °C). Considering the amphibole aluminum geobarometer which is suitable for granitic rocks, very similar results are provided according the different authors (Table 5; Hammarstrom and Zen, 1986; Holluster et al., 1987; Johnson et al., 1989, Schmidt, 1992). Usually, the pressure estimate given by Schmidt (1992) is considered to be adapted to our mylonitic granodiorite (Ratschbacher, 2000) which gives an average pressure of 0.74±0.05 GPa (Table 5; Fig. 8). Relatively, the thermobarometers of Holdaway (2000) and Wu et al. (2004) could give more accurate P-T values, as the same activity models for garnet and biotite in Grt-Bt thermometer (Holdaway, 2000) and Grt-Bt-Pl-Qtz barometer (Wu et al., 2004) are applied respectively, and the garnet, biotite and plagioclase seems have not been influenced by later metamorphism. Hence, the peak P-T conditions appraised by the thermobarometers from Holdaway (2000) and Wu et al. (2004) maybe close to the more real 'peak' P-T conditions, and an average P-T values with standard deviation of 569±8 °C and 0.87±0.04 GPa is estimated.

Assuming a rock density of 2800 kg/m^3 in average (Ratschbacher et al., 2000; Zheng, 1997), this Jurassic granitoid emplaced around 26-31 km depth. This result is in agreement with the granite geochemistry. A low (^{87}Sr / ^{86}Sr)i ratio and high εNd(t) value indicate that the Jurassic plutons originated from the partial melting of the lower part of a juvenile crust (Wu et al., 2005b). If this interpretation is correct, the temperature gradient in the Jurassic crust was about 20 °C/Km. Such a value complies with the thermal gradient derived from the vitrinite reflectance (Ro) of Mesozoic sedimentary basin of North China and indicated research area has analogous to stable cratonic crust during Jurassic to Early Cretaceous (Fu et al., 2005; Zhai et al., 2004)

5.2. A two phases cooling history for the south Liaodong peninsula MCC

The Jurassic granodiorite and Cretaceous monzogranite show very different cooling histories (Fig. 9). This indicates that the granitic and metamorphic rocks in the south Liaodong peninsula MCC experienced at least two distinct exhumation stages. South of Pulandian city, in the footwall of the detachment normal fault, zircon and titanite yield U/Pb ages of 170-177 Ma and 160 Ma respectively (Wu et al., 2005b; Yang et al., 2007a; Fig. 3). The hornblende ^{40}Ar/^{39}Ar ages of 121.7-116 Ma obtained from the mylonitized granodiorite allow us to derive a cooling rate of about 3°C/My from zircon crystallization temperatures of ca. 700-800 °C, passing the titanite crystallization temperatures of ca. 630°C, to hornblende closure temperature of ca. 550°C (Fig. 9). On the contrary, the Cretaceous monzogranite yield U/Pb zircon ages around 128-118 Ma (Wu et al., 2005a), biotite and K-feldspar ^{40}Ar/^{39}Ar ages obtained from the pluton host rocks at 113-111Ma and 118-112 Ma respectively (Fig. 3; Yang et al., 2007b). Combined with amphibole ages of the Jurassic granodiorite (Fig. 9), the cooling rate is about 40-55 °C/My (Fig. 9). This result showing a fast cooling for the south Liaodong MCC is in agreement with the previous works on metamorphic core complex and syn-tectonic granite reported in Eastern China (Ratschbacher et al., 2000; Yang et al., 2004, 2007b, 2008; Wang and Li, 2008). Because of the lack of mineral with closure temperature between titanite and amphibole (i.e. 630-550°C), we cannot precisely estimate the cooling and exhumation history during 160-122 Ma interval. Four possibilities are suggested here.

(1) *Slow cooling*. Considering the zircon and titanite U/Pb, and the hornblende ^{40}Ar/^{39}Ar ages, a slow cooling rate of about 3°C/My can be derived. This means that

during ca. 40 Ma, from 160 Ma to 122 Ma, the crust of the Liaodong peninsula remained rather stable and thermally undisturbed until the emplacement of Cretaceous plutons.

(2) *Slow cooling and Cretaceous reheating*. Alike in other places of eastern part of NCC, the Early Cretaceous is a period of intense plutonism during which the crust reached a high temperature (Zhai et al., 2004). This reheating event will influence the cooling history of the Jurassic plutons. Such a reheating effect during the Early Cretaceous is suggested in the cooling path drawn on Fig. 9. A similar thermal overprint has been reported in the Dabieshan and Lushan areas (Faure et al., 2003a; Lin et al., 2000).

(3) *Slow cooling and progressive reheating*. The 10°C/Ma cooling rate indicated by zircon and titanite U/Pb ages from the Jurassic granodiorite, is progressively modified since Early Cretaceous by a continuous emplacement of large masses of granitic plutons that reheat the crust of the south Liaodong peninsula.

(4). *Two pulses of syntectonic plutonism*. During the Jurassic (before 150 Ma, fig. 9A), the granodiorite experienced a 10°C/Ma cooling rate that led to a rather “cool” crust, then since Early Cretaceous, the emplacement of a huge amount of granitoid magma was responsible for reheating of the entire crust. This last possibility of cooling path of the South Liaodong peninsula is in agreement with the suggestion of NCC lithosphere removal commencing as soon as Jurassic (Griffin et al., 1998; Gao et al., 2004). In this view, a fast cooling rate similar to the early Cretaceous one must be taken into account. At the scale of NE China, the Mesozoic plutonism distributes in two distinct pulses of Jurassic and Cretaceous age (Wu et al., 2005a, b; Fig. 9A), but in the present state of knowledge, the tectonic setting of the Jurassic magmatism is not settled yet. If Jurassic extensional tectonics is assumed, as suggested by the grabens distributed in the Liaoning Province (LBGMR, 1989), the Jurassic plutons might be interpreted as syn-kinematic bodies and a fast cooling rate will follow the emplacement of these plutons. During the Early Cretaceous, the crust was progressively reheated due to the emplacement of the Early Cretaceous monzogranitic plutons and this event is coeval with an intensive extensional tectonics (Lin and Wang, 2006; Lin et al., 2008b).

No mater what cooling history is taken into consideration, our results indicate a very complex tectonic evolution during Late Jurassic to Early Cretaceous for the South Liaodong peninsula. Because the extensional structures are not quite significantly developed despite the presence of some Jurassic basins, the last possibility (path 4) seems unlikely (Fig. 9; LBGMR, 1989). The first and second ones imply the presence of a relatively "hot" crust and high heat flow during the entire Jurassic period. However, this is inconsistent with the recent evaluation of heat flow and thermal gradient that does not argue for this Jurassic "hot" crust (Zhai et al., 2004). In the Jurassic granodiorite, the garnet does not show a clear zonal structure, while amphibole develops a retrograde zonation. This suggests that this granodiorite experienced a simple thermal evolution such as that depicted as path 3 in figure 9. Whatever the Late Jurassic- Early Cretaceous cooling paths, a rapid cooling rate took place during the Late Early Cretaceous subsequently to the extensional emplacement of the monzogranitic plutons (116-122Ma). A similar result was indicated by the Gudaoling syntectonic granite which situated north part of the south Liaodong peninsula MCC (Fig. 9). If the path 3 is acceptable, it will reveal that, at least in south Liaodong peninsula, the extensional tectonics was not significant before Early Cretaceous. This cooling path recorded by the south Liaodong peninsula MCC indicate two contrasted processes of the crustal evolution of NCC during the Late Mesozoic (Wu et al., 2005a, 2005b).

5.3. The significance of rapid exhumation and regional extension along the Eastern Margin of Eurasia

Previous structural works show that the south Liaodong peninsula massif is an asymmetric MCC with a NE-SW trending extension direction (Liu et al., 2005; Yang et al., 2007b; Lin et al., 2008b). Due to movements along detachment faults, the Jurassic granodioritic plutons, Paleoproterozoic and Archean country rocks were brought to the surface in the core of MCC. The ^{40}Ar/ ^{39}Ar ages constrain the age of the ductile extension around 120 Ma. In the mean time, these exhumed rocks recorded at least two different paths of cooling that are poorly documented in the other MCCs (Ratschbacher et al., 2000; Yang et al., 2007b). In the south Liaodong peninsula MCC, these two different cooling histories correspond to different exhumation and geodynamic processes. The mechanism of lithosphere removal responsible for the Cretaceous reheating of the crust is still controversial (c.f. Lin and Wang, 2006 and reference therein). The progressive thermo-mechanical convective ablation of the lithosphere, as suggested for the North American Cordilleras (Bird, 1979), was accepted by some workers (Griffin et al., 1998; Menzies and Xu, 1998; Xu, 2001). But such a mechanism cannot satisfactorily explain the peak of the magmatism and extensional structures (MCC, syntectonic pluton, half graben basin etc…) of early Cretaceous age (Fig. 10). Alternatively, another possible mechanism that can be invoked is the detachment of a large piece of lithosphere (Houseman et al., 1981). Because it gives answer to many of the above questions about the thermal evolution of Eastern China, this lithosphere delamination model was well accepted by most of researchers (Deng et al., 1994, 1996; Wu et al., 2000, 2003; Gao et al., 1998, 2002). Nevertheless, whatever the model, the partial loss of mantle would be also responsible for a significant uplift and rise of a high elevation plateau like in Tibet (Turner et al., 1996). Although such a Cretaceous plateau is suggested for Mongolia and NE China (Meng et al., 2003), this topographic effect is not well recorded in the sedimentation since the amount of terrigeneous material deposited in the Cretaceous basins does not comply with the important erosion associated to such an uplift. The slow cooling history recorded by the Jurassic granodiorite does not support the delamination model during the Jurassic (Griffin et al. 1998; Gao et al. 2004), at least in the Liaodong Peninsula area. A detail discussion of the models of lithosphere removal is beyond the scope of this paper. In the present state of knowledge, we consider that additional structural and cooling data on exhumed rocks from extensional domes are necessary to reach a satisfactory understanding of the geodynamic significance of the continental-scale Mesozoic extension in the North China Craton.

6. Conclusion

The south Liaodong Peninsula MCC, which is the easternmost extensional dome recognized in Eastern China, provides a good example of structure combining synmetamorphic ductile shearing, synkinematic plutonism and polyphase exhumation. The Jurassic granodioritic plutons recorded two different phases of cooling. A slow cooling regime at about 3-10°C/My before 122 Ma and a fast cooling rate at about 40-55 °C/My after 122 Ma. This result indicates that this Jurassic granodiorite which belongs to the footwall of the detachment normal faults, experienced two different exhumation processes during the Mesozoic: a Jurassic slow or negligible uplifting followed by Cretaceous quite fast exhumation. These two different cooling histories correspond to a significant change of the geodynamical evolution of Eastern China between the Jurassic and Cretaceous.

Acknowledgements

Field and laboratory expenses have been supported by a Knowledge Innovtion Program of the Chinese Academy of Sciences (KZCX2-YW-Q05-05-03) and NSFC (40872142, 90714007). Constructive comments by Drs. S. Wilde, Pierre Vergely and Bin Chen on this draft are deeply acknowledged. We also thank Prof. Bor-ming Jahn for his helpful editorial advice.

References

Allen, M.B., Macdonald, D.I., Zhao, X., Vincent, S., Brouet-Menzies C., 1997. Early Cenozoic two-phase extension and late Cenozoic thermal subsidence and inversion of the Bohai Basin, Northern China. Marine and Petroleum Geology 14, 951-972.

Bird, P., 1979. Continental delamination and the Colorado Plateau. Journal of Geophysical Research 84, 7561-7571.

Cheng, R.Y., Wu, F.Y., Ge, W., Sun, D., Liu, X., Yang, J., 2006. Emplacement age of the Raohe Complex in eastern Heilongjiang province and the tectonic evolution of the eastern part of Northeastern China. Acta Petrologica Sinica 22, 315-325 (In Chinese with English abstract).

Dahl, P.S., 1996. The effects of composition on retentivity of argon and oxygen in hornblende and related amphiboles: a field-tested empirical model. Geochimica et Cosmochimica Acta 60, 3687-3700.

Davis, G.A., Zheng, Y., Wang, C., Darby, B.J., Zhang, Ch., Gehrels, G.E., 2001. Mesozoic tectonic evolution of the Yanshan fold and thrust belt, with emphasis on Hebei and Liaoning provinces, northern China, In Hendrix, M.S., Davis, G.A. (Eds.), Paleozoic and Mesozoic tectonic evolution of Central and Asia: From Continental Assembly to Intracontinental Deformation. Boulder, Colorado, Geological Society of American Memoir 194, pp.171-194.

Deng, J., Mo, X., Zhao, H., Wu, Z., Luo, Z., Su, S., 2004. A new model for the dynamic evolution of Chinese lithosphere: ‘continental roots-plume tectonics’. Earth Science Reviews 65, 223-275.

Deng, J., Zhao, H., Luo, Z., Guo, Z., Mo, X., 1998. Mantle plumes and lithosphere motion in East Asia, In: Flower, M.F.J., Chung, S.L., Lo, C.H., Lee, T.Y. (Eds.), Mantle Dynamics and Plate Interaction in East Asia. Geodynamics Series 27, pp. 59-66.

Deng, J.F, Mo, X.X., Zhao, H.L., Luo, Z.H., Du, Y.S, 1994. Lithosphere root/de-rooting and activation of the East China continent. Geoscience 8, 349-356 (in Chinese, with English abstract).

Deng, J.F, Zhao, H.L., Mo, X.X., 1996. Continental Roots-Plume Tectonics of China: Key to Continental Dynamics. Geological Pubulishing House, Beijing, pp. 1-110 (in Chinese, with English abstract).

Fan, W.M., Menzies, M.A., 1992. Destruction of aged lower lithosphere and asthenosphere mantle beneath eastern China. Geotectonica et Metallogenia 16, 171-179 (In Chinese with English abstract).

Faure, M., Lin, W., Monié, P., Bruguier, O., 2004. Paleoproterozoic collision tectonics in NE China: evidence for a 2Ga magmatic arc in Liaodong Peninsula. Terra Nova 16, 75-80.

Faure, M., Lin, W., Monié, P., Le Breton, N., Poussineau, S., Panis, D., Deloule, E., 2003a. Exhumation tectonics of the ultra high-pressure metamorphic rocks in the Qinling orogen in East China. New petrological-structural-radiometric insights from the Shandong peninsula. Tectonics 22, 1018-1039.

Faure, M., Lin, W., Scharer, U., Shu, L., Sun, Y., Arnaud, N., 2003b. Continental subduction and exhumation of UHP rocks. Structural and geochronological insights from the Dabieshan (East China). Lithos 70, 213-241.

Faure, M., Trap, P., Lin, W., Monié, P., Bruguier, O., 2007. Polyorogenic evolution of the Paleoproterozoic Trans-North China Belt, new insights from the Lüliangshan-Hengshan-Wutaishan and Fuping massifs. Episodes 30, 95-106.

Fleck, R.J, Sutter, J.F., Elliot, D.H., 1977. Interpretation of discordant ^{40}Ar/ ^{39}Ar age-spectra of Mesozoic tholeiites from Antarctica. Geochimica et Cosmochimica Acta 41, 15-32.

Fu, M., Hu, Sh., Wang, J., 2005. Thermal regime transition in eastern North China and its tectonic implication. Science in China (Series D) 48, 840-848.

Gao, S., Rudnick, R.L., Yuan, H.L., Liu, X.M., Liu, Y.S., Xu, W.L., Ling, W.L., Ayers, J., Wang, X.C., Wang, Q.H., 2004. Recycling lower continental crust in the North China craton. Nature 432, 892-897.

Gao, S., Rudnick, R.L., Carlsonet, R.W., McDonough, W.F., Liu, Y.S., 2002. Re-Os evidence for replacement of ancient mantle lithosphere beneath the North China Craton. Earth and Planetary Science Letters 198, 307-322.

Gao, S., Zhang, B.-R., Jiu, Z.-M., Kern, H., Luo, T.-C., Zhao, Z.-D., 1998. How mafic is the lower continental crust? Earth and Planetary Science Letters 161, 101-117.

Griffin, W., Zhang, A., O'Reilly, S., Ryan, C.G., 1998. Phanerozoic evolution of the lithosphere beneath the Sino-Korean Craton, In: Flower, M.F.J., Chung, S.L., Lo, C.H., Lee, T.Y. (Eds.), Mantle Dynamics and Plate Interaction in East Asia. Geodynamics Series 27, pp. 107-126.

Hacker, B.R., Ratschbacher, L., Webb, L., Ireland, T., Walker, D., Dong, S., 1998. U/Pb zircon ages constrain the architecture of the ultrahigh-pressure Qinling-Dabie orogen, China. Earth and Planetary Science Letters 161, 215-230.

Hacker, B.R., Wallis, S.R., Ratschbacher, L., Grove, M., Gehrels, G., 2006. High-temperature geochronology constraints on the tectonic history and architecture of the ultrahigh-pressure Dabie-Sulu Orogen. Tectonics 25, doi: 10.1029/2005TC001937.

Hammarstrom, J. M., Zen, E., 1986. Aluminum in hornblende: An empirical igneous geobarometer. American Mineralogist 71, 1297-1313.

Harrison, T.M., Duncan, I., McDougall, I., 1985. Diffusion of ^{40}Ar in biotite: Temperature, pressure and compositional effects. Geochimica et Cosmochimica Acta 49, 2461-2468.

HBGMR (Hebei Bureau of Geology and Mineral Resources), 1989. Regional Geology of Hebei Province, Geological Publishing House, Beijing, 742 pp (In Chinese with English abstract).

Hermann, J., 2002. Allanite: thorium and light rare earth element carrier in subducted crust, Chemical Geology 192, 289-306.

Holdaway, M.J., 2000. Application of new experimental and garnet Margules data to the garnet-biotite geothermometer. American Mineralogist 85, 881-892.

Hollister, L.S., Grissom, G.C., Peters, E.K., Stowell, H.H., Sisson, V.B., 1987. Confirmation of solidification of calc-alkaline plutons. American Mineralogist 72, 231-239.

Houseman, G., McKenzie, D. P., Molnar, P., 1981. Convective instability of a thickened boundary layer and its relevance for the thermal evolution of continental convergent belts. Journal of Geophysical Research 86, 6115-6132.

Huang, T. K., 1945. On the major tectonic forms of China. Geological Memories, Series A, 20, pp 1-165.

Jiang, N., Sun, Sh., Zhu, X., Mizuta, T., Ishiyama, D., 2003. Mobilization and enrichment of high-field strength elements during late- and post-magmatic processeds in the Shuiquangou syenitic complex, Northern China. Chemical Geology 200, 117-128.

Johnson, M.C., Malcolm, J., Rutherford, J., 1989. Experimental calibration of the aluminum-in-hornblende-geobarometer with application to Long Valley caldera (California) volcanic rocks. Geology 17, 837-841.

Kohn, M.J., Spear, F.S., 1990. Two new geobarometers for garnet amphibolites, with application to southeastern Vermont. American Mineralogist 75, 89-96.

Krogh, T.E., 1982. Improved accuracy of U-Pb zircon ages by the creation of more concordant system using air abrasion technique. Geochimica et Cosmochimica Acta 46, 637-649.

Krogh-Ravna, E., 2000. Distribution of Fe^{2+} and Mg between coexisting garnet and hornblende in synthetic and natural systems: an empirical calibration of the garnet-hornblende Fe-Mg geothermometer. Lithos 53, 265-277.

Kusky, T.M., Li, J.H., 2003. Paleoproterozoic tectonic evolution of the North China Craton. Journal of Asian Earth Sciences 22, 383-397.

Lamb, M.A., Badarch, G., 1997. Paleozoic sedimentary basins and volcanic-arc systems of southern Mongolia: New stratigraphic and sedimentological constraints. International Geology Review 39, 542-576.

LBGMR (Liaoning Bureau of Geology and Mineral Resources), 1989. Regional Geology of

Liaoning Province, Geological Publishing House, Beijing, 856 pp (In Chinese with English summary).

Leake, B.E., Woolley, A.R., Arps, C.E.S., Birch, W.D., Gilbert, M.C., Grice, J.D., Hawthorne, F.C., Kato, A., Kisch, H.J., Krivovichev, V.G., Laird, J., Mandarino, J.A., Maresch, W.V., Nickel, E.H., Rock, N.M.S., Schumacher, J.C., Smith, D.C., Stephenson, N.C.N., Ungaretti, L., Whittaker, E.J.W., Guo, Y., 1997. Nomenclature of amphiboles: report of the subcommittee on amphiboles of the international mineralogical association, commission on new minerals and mineral names. The Canadian Mineralogist 35, 219-246.

Li, S., Zhao, G., Sun, M., Han, Zh., Luo, Y., Hao, D., Xia, X., 2005. Deformation history of the Paleoproterozoic Liaohe assemblage in the eastern block of North China Craton. Journal of Asian Earth Sciences 24, 659-674.

Lin, W., Faure, M., Monié, P., Schärer, U., Zhang, L., Sun, Y., 2000. Tectonics of SE China, new insights from the Lushan massif (Jiangxi Province). Tectonics 19, 852-871.

Lin, W., Faure, M., Nomade, S., Shang, Q., Renne, P.R., 2008a. Permian-Triassic Amalgamation of Asia: insights from NE China sutures and their place in the final collision of North China and Siberia. Comptes Rendus Geoscience 340, 190-201.

Lin, W., Faure, M., Monie, P., Scharer, U., Panis, D., 2008b. Mesozoic extensional tectonics in Eastern margin of Eurasia continent, the case study of South-Liaodong peninsula dome, NE China. Journal of Geology 116, 134-154.

Lin, W., Wang, Q., 2006. Late Mesozoic extensional tectonics in North China Block - Response to the Lithosphere removal of North China Craton? Bulletin de la Société

Géologique de France 177, 287-294.

Lister, G.S., Davis, G.A., 1989. The origin of metamorphic core complexes and detachment faults formed during Tertiary continental extension in the northern Colorado River region, U.S.A. Journal Structural Geology 11, 65-94.

Liu, J., Davis, G., Lin, Z., Wu, F., 2005. The Liaonan metamorphic core complex, Southeastern Liaoning Province, North China: A likely contributor to Cretaceous rotation of Eastern Liaoning, Korea and contiguous areas. Tectonophysics 407, 65-80.

Lu, X., Wu, F., Lin, J., Sun, D., Zhang, Y., Guo, C., 2004. Geochronological successions of the Early Precambrian granitic magmatism in Southern Liaodong peninsula and it constraints on tectonic evolution of the north China Craton. Chinese Journal of Geology 39, 123-138 (In Chinese with English abstract).

Mattauer, M., Matte, P., Malavieille, J., Tapponnier, P., Maluski, H., Xu, Z., Lu, Y., Tang, Y., 1985. Tectonics of Qinling belt: Build-up and evolution of eastern Asia. Nature 317, 496-500.

McDougall, I., Harrison, T.M., 1999. Geochronology and Thermochronology by the ^{40}Ar/^{39}Ar Method, Oxford University Press, New York, Oxford, 269pp.

Meng, Q., 2003. What drove late Mesozoic extension of the northern China-Mongolia tract? Tectonophysics 369, 155-174.

Meng, Q., Hu, J., Jin, J., Zhang, Y., Xu, D., 2003. Tectonics of the late Mesozoic wide extension basin system in the China-Mongolia border region. Basin Research 15, 397-415.

Menzies, M.A., Xu, Y., 1998. Geodynamics of the North China Craton. in: Mantle Dynamics and Plate Interaction in East Asia. . In: Flower, M.F.J., Chung, S.L., Lo, C.H., Lee, T.Y. (Eds.), Mantle Dynamics and Plate Interaction in East Asia. Geodynamics Series 27, pp. 155-165.

Menzies, M.A., Fan, W.M., Zhang, M., 1993. Palaeozoic and Cenozoic lithoprobes and the loss of >120 km of Archean lithosphere, Sino-Korean craton, China, In Prichard, H.M., Alabaster, T., Harris, N.B.W., Neary, C.R., (Eds.), Magmatic Processes and Plate Tectonics. Geological Society of London Special Publication 76, 71-81.

Okada, H., 1999. Plume-related sedimentary basins in East Asia during the Cretaceous. Paleogeography, Paleoclimatology, Paleoecology 150, 1-11.

Okamoto, K., Maruyama, S., 1999. The high-pressure synthesis of lawsonite in the MORB + H_2O system. American Mineralogist 84, 362-373.

Ratschbacher, L., Hacker, B.R., Webb, L., McWilliams, M.O., Ireland, T., Dong, S., Calvert, A., Chateigner, D., Wenk, H., 2000. Exhumation of ultrahigh-pressure continental crust in east central China: Cretaceous and Cenozoic unroofing and the Tan-Lu fault. Journal of Geophysical Research 105, 13303-13338.

Ren, J., Kensaku, T., Li, S., Zhang, J., 2002. Late Mesozoic and Cenozoic rifting and its dynamic setting in Eastern China and adjacent areas. Tectonophysics 344, 175-205.

Samson, S.C., Alexander, E.C., 1987. Calibration of the inter laboratory ^{40}Ar/^{39}Ar dating standard MMHb-1. Chemical Geology 66, 27-34.

SBGMR (Shanxi Bureau of Geology and Mineral Resources), 1989. Regional Geology of Shanxi Province, Geological Publishing House, Beijing, 780 pp.

Schärer, U., 1984. The effect of initial ^{230}Th disequilibrium on young U-Pb ages, the Makalu case, Himalaya. Earth and Planetary Science Letters 67, 101-114.

Schärer, U., Labrousse, L., 2003. Dating the exhumation of UHP-rocks and associated crustal melting in the Norwegian Caledonides. Contributions to Mineralogy and Petrology 144, 758-770.

Schmidt, M.W., 1992. Amphibole composition in tonalite as a function of pressure: an experimental calibration of the Al-in-hornblende barometer. Contributions to Mineralogy and Petrology 110, 304-310.

Sengor, A.M.C., Natal'in, B.A., 1996. Paleotectonics of Asia: fragments of a synthesis, In: Yin, A., Harrison, T.M. (Eds.), The Tectonic Evolution of Asia. Cambridge University Press, pp. 486-641.

Shang, Q., 2004. Occurrences of Permian radiolarians in central and eastern Nei Mongol (Inner Mongolia) and their geological significance to the Northern China Orogen. Chinese Science Bulletin 49, 2613-2619.

Stacey, J.S, Kramers, J.D., 1975. Approximation of terrestrial lead isotope evolution by a two stage model, Earth and Planetary Science Letters 26, 207-221.

Tian, Z., Han, P., Xu, K., 1992. The Mesozoic-Cenozoic east China rift system. Tectonophysics 208, 341-363.

Trap, P., Faure, M., Lin, W., Monié, P., 2007. Late Paleoproterozoic (1900-1800 Ma) nappe stacking and polyphase deformation in the Hengshan-Wutaishan area: implications for the understanding of the Trans-North-China Belt, North China Craton. Precambrian Research 156, 85-106

Turner, S., Arnaud, N., Liu, J., Rogers, N., Hawkesworth, C., Harris, N., Kelley, S., van Calsteren, P., Deng, W., 1996. Post-collision, shoshonitic volcanism on the Tibetan Plateau implications for convective thinning of the lithosphere and the source of ocean island basalts. Journal of Petrology 37, 45-71.

Wang, Q., Liu X., 1986. Paleoplate tectonics between Cathaysia and Angaraland in Inner Mongolia of China. Tectonics 5, 1073-1088.

Wang, Y., Li, H., 2008. Initial Formation and Mesozoic Tectonic Exhumation of an Intracontinental Tectonic Belt of the Northern Part of the Taihang Mountain Belt, Eastern Asia. The Journal of Geology 116, 155–172.

Wu, C.H., Zhang, J., Ren, L.D., 2004. Empirical Garnet-Biotite-Plagioclase-Quartz (GBPQ) Geobarometry in Medium- to High-Grade Metapelites. Journal of Petrology 45, 1907-1921.

Wu, F.Y., Yang, J.H., Zhang, Y.B., 2006. Emplacement ages of the Mesozoic granites in southeastern part of the Western Liaoning Province. Acta Petrologica Sinica 22, 315-325 (In Chinese with English abstract).

Wu, F., Lin, J., Wilde, S.A., Zhang, X., Yang, J., 2005a. Nature and significance of the Early Cretaceous Giant Igneous Event in Eastern China. Earth and Planetary Science Letters 233, 103-119.

Wu, F., Yang, J., Wilde, S.A., Zhang, X., 2005b. Geochronology, petrogenesis and tectonic implications of the Jurassic granites in the Liaodong Peninsula, NE China. Chemical Geology 221, 127-156.

Wu, F.Y., Han, R.H., Yang, J.H., Wilde, S.A., Zhai, M.G., 2007. Initial constraints on granitic magmatism in North Korea using U-Pb zircon geochronology. Chemical Geology 238, 232-248.

Wu, F.Y., Jahn, B.M., Wilde, S.A, Sun, D.Y., 2000. Phanerozoic continental crustal growth: U-Pb and Sr-Nd isotopic evidence from the granites in northeastern China. Tectonophysics 328, 89-113.

Wu, F.Y., Jahn, B.M., Wilde, S.A., Lo, C.H., Yui, T.F., Lin, Q., Ge, W.C., 2003. Highly fractionated I-type granites in NE China (I): geochronology and petrogenesis. Lithos 66, 241-273.

Xiao, W., Windley, B.F., Hao, J., Zhai, M., 2003. Accretion leading to collision and the Permian Solonker suture, Inner Mongolia, China: Termination of the Central Asian orogenic belt. Tectonics 22, Doi:10.1029/2002TC001484.

Xu, Y.G., 2001, Thermo-tectonic destruction of the Archean lithospheric keel beneath the Sino - Korean craton in China: evidence, timing and mechanism. Physics and Chemistry of the Earth 26, 747-757.

Xu, Y.G., 1999. Roles of thermo-mechanic and chemical erosion in continental lithospheric thinning. Bulletin of Mineralogy Petrology and Geochemistry 18, 1-5 (in Chinese with English abstract).

Yang, J.H., Wu, F.Y., Chung, S.L., Lo, Ch.H., 2008. The extensional geodynamic setting of Early Cretaceous granitic intrusions in the eastern North China Craton: Evidence from laser ablation $^{40}Ar/^{39}Ar$ dating of K-bearing minerals. Acta Petrologica Sinica, 24, 1175-1184 (In Chinese with English abstract)

Yang, J.H., Wu, F., Liu X., Xie L., Yang Y., 2007a. Petrogenesis and geological significance of the Jurassic Xiaoheishan pluton in the Liaodong peninsula, East China: In-situ zircon U-Pb dating and Hf isotopic analysis. Bulletin of Mineralogy Petrology and Geochemistry 126, 29-43.

Yang, J.H., Wu, F.Y., Chung, S.L, Lo, Ch., Wilde, S.A., Davis, G.A., 2007b. Rapid exhumation and cooling of the Liaonan metamorphic core complex: Inferences from $^{40}Ar/^{39}Ar$ thermochronology and implications for Late Mesozoic extension in the eastern North China Craton. Geological Society of America Bulletin 119, 1405-1414.

Yang, J.H., Sun, J.F., Chen, F.K., Wilde, S.A., Wu, F.Y., 2007c. Sources and petrogenesis of Late Triassic dolerite dikes in the Liaodong Peninsula: Implications for post-collisional lithosphere thinning of Eastern North China Craton. Journal of Petrology 48, 1973-1997.

Yang, J.H., Wu, F.Y., Shao, J.A., Xie, L., Liu, X., 2006. In-Situ U-Pb dating and Hf isotopic analyses of zircon from volcanic rocks of the Houcheng and Zhangjiakou formations in the Zhang-Xuan Area, Northeast China. Earth Science-Journal of China University of Geosciences 31, 71-80 (In Chinese with English abstract).

Yang, J.H., Wu, F.Y., Lo, Ch.H., Chung, S.L., Zhang, Y.B., Wilde, S.A., 2004. Deformation age of Jurassic granites in the Dandong area, eastern China: $^{40}Ar/^{39}Ar$ geochronological constraints. Acta Petrologica Sinica, 20, 1205-1214 (In Chinese with English abstract).

Yin, A., Nie, S., 1993. An Indentation model for the North and South China collision and the development of the Tan-lu and normal fault systems, Eastern Asia. Tectonics 12, 801-813.

Yin, A., Nie, S., 1996. A Phanerozoic palinspastic reconstruction of China and its neighboring regions, In: Yin, A., Harrison, T.M. (Eds.), The Tectonic Evolution of Asia. Cambridge University Press, pp. 442-485.

Zartman, R.E., Doe, B.R., 1981. Plumbotectonics, the model. Tectonophysics 75, 135-162.

Zhai, M., Zhu, R., Liu, J., Meng, Q., Hou, Q., Hu, S., Liu, W., Li, Zh., Zhang, H., 2004. Time range of Mesozoic tectonic regime inversion in eastern North China Block. Science in China (Series D) 47, 151-159.

Zhang, H.F., 2005. Transformation of lithospheric mantle through peridotite-melt reaction: A case of Sino-Korean craton. Earth and Planetary Science Letters 237, 768-780.

Zhang, H.F., Zheng, J.P., 2003. Geochemical characteristics and petrogenesis of Mesozoic basalts from the North China Craton: A case study in Fuxin, Liaoning Province. Chinese Science Bulletin 48, 924-930.

Zhang, H.F., Sun, M., 2002. Geochemistry of Mesozoic basalts and mafic dikes in southeastern North China craton, and tectonic implication. International Geological Review 44, 370-382.

Zhang, L.S., Schärer, U., 1996. Inherited Pb components in magmatic titanite and their consequence for the interpretation of U-Pb ages. Earth and Planetary Science Letters 138, 57-65.

Zhao, G., Sun, M., Wilde, S.A., Li, S.Z., 2005. Late Archean to Paleoproterozoic evolution of the North China Craton: key issues revisited. Precambrian Research 136, 177-202.

Zheng, X., 1997. Characteristics and geological significance of deep tectonics in Liaoning

Province. Liaoning Geology 3, 16-38.

Zorin, Y.A., 1999. Geodynamics of the western part of the Mongolia-Okhotsk collisional belt, Trans-Baikal region (Russia) and Mongolia. Tectonophysics 306, 33-56.

Figure captions

Fig. 1. Regional-scale structural map of the South Liaodong Peninsula massif. Inset shows the location of study area within the broader context of East Asia (Modified from Lin et al., 2008b). NCB, North China Block; SCB, South China Block.

Fig. 2. Cross-sections though the South Liaodong Peninsula massif (location shown in Fig. 1) drawn parallel to the direction of the main mineral and stretching lineation (Modified from Lin et al., 2008b).

Fig. 3. Map of the South Liaodong Peninsula massif showing the available radiometric data. $^{40}Ar/^{39}Ar$ ages of biotite and amphibole and U/Pb age of titanite are given in this paper. ICP-MS, SHRIMP and TIMS zircon ages are from Wu et al. (2005a, 2005b), Ar-biotite and muscovite ages from Yin & Nie (1996) and K-feldspar ages from Yang et al. (2007b). Symbols and captions in the map are the same as in figure 1.

Fig. 4. $^{40}Ar/^{39}Ar$ ages spectra of biotite (a to e) and amphibole (f to i), from gneissic migmatites, amphibolite, orthogneiss, mylonitic and undeformed granite from South Liaodong Peninsula massif

Fig. 5. U/Pb concordia diagram of titanite fractions from the granodiorite (sample LN 82)

Fig. 6. (A) AlKα, (B) CaMα, (C) FeKα (D) MnKα X-ray mapping images of garnet, (E) step

scanning analyses and (F) chemical composition of anhedral garnet of Jurassic granodiorite that involved into the exhumation of South-Liaodong Peninsula massif. Warmer color indicates higher concentration of element. Abbreviations of end-members are: alm, almandine; sps, spessartine; prp, pyrope; grs, grossular

Fig. 7. A and B. Chemical composition and profile of amphibole in the Jurassic granodiorite. Grids dividing the composition space after Leake (1997); C. Chemical composition of feldspar of Jurassic granodiorite. Abbreviations of end-members are: Ab: Albite; An: Anorthite; Or: Orthoclase. (D) AlKα, (E) CaMα and (F) FeKα X-ray mapping images of the chemical composition of anhedral allanite and rimed epidote in the Jurassic granodiorite involved into the exhumation of South-Liaodong Peninsula massif. Warmer and bright colors indicate higher concentration of element.

Fig. 8. *P-T* diagram showing the peak metamorphic *P-T* conditions for the garnet-bearing Jurassic gneissic granodiorite involve into the exhumation showing the evolution of the South-Liaodong Peninsula MCC based on the different thermobarometers. Metamorphic facies grid is from Okamoto & Maruyama (1999). (Black cross shows the average of standard deviation), BS: Blueschist; EA: Epidote-amphibolite; GS: Greenschist; AM: Amphibolite; Amp-Ec: Amphibolite-eclogite; HGR: High temperature granulite; LGR: Low temperature granulite.

Fig. 9. Possible cooling paths of the south Liaodong Peninsula massif. Plain line corresponds to the Cretaceous cooling after 550°C, different dashed line indicates the different possibilities of cooling history of the deformed Jurassic pluton. Path 1 corresponds to a slow cooling rate (3 °C/My) followed by a fast cooling (40-55 °C/My). Path 2 corresponds to an Early Cretaceous thermal pulse overprinted upon cooled Jurassic plutons. Path 3 corresponds to slow cooling rate (10 °C/My) and progressive reheating

by an Early Cretaceous thermal pulse overprinted upon the Jurassic cooling trend. Path 4 corresponds to two pulses of syn-kinematic plutonism. The Late Jurassic granodiorite experienced a fast cooling rate related to its syn tectonic emplacement. In Early Cretaceous time, the new plutonic pulse reheated the already cooled Jurassic pluton and its country rocks. Inset shows the age distribution of the Mesozoic igneous rocks in eastern China and North Korea (n =393). Two important periods of magmatism are shown, namely a Cretaceous peak at ca. 125 Ma and a more scattered Jurassic plutonism for 195 Ma to 155 Ma (from Davis et al., 2001; Cheng et al., 2006; Yang et al., 2004, 2006, 2008; Wu et al. 2005a, 2005b, 2006, 2007).

Fig. 10. Schematic diagram of the south Liaodong Peninsula massif showing regional extensional structures (MCC, syntectonic pluton and half graben basins).

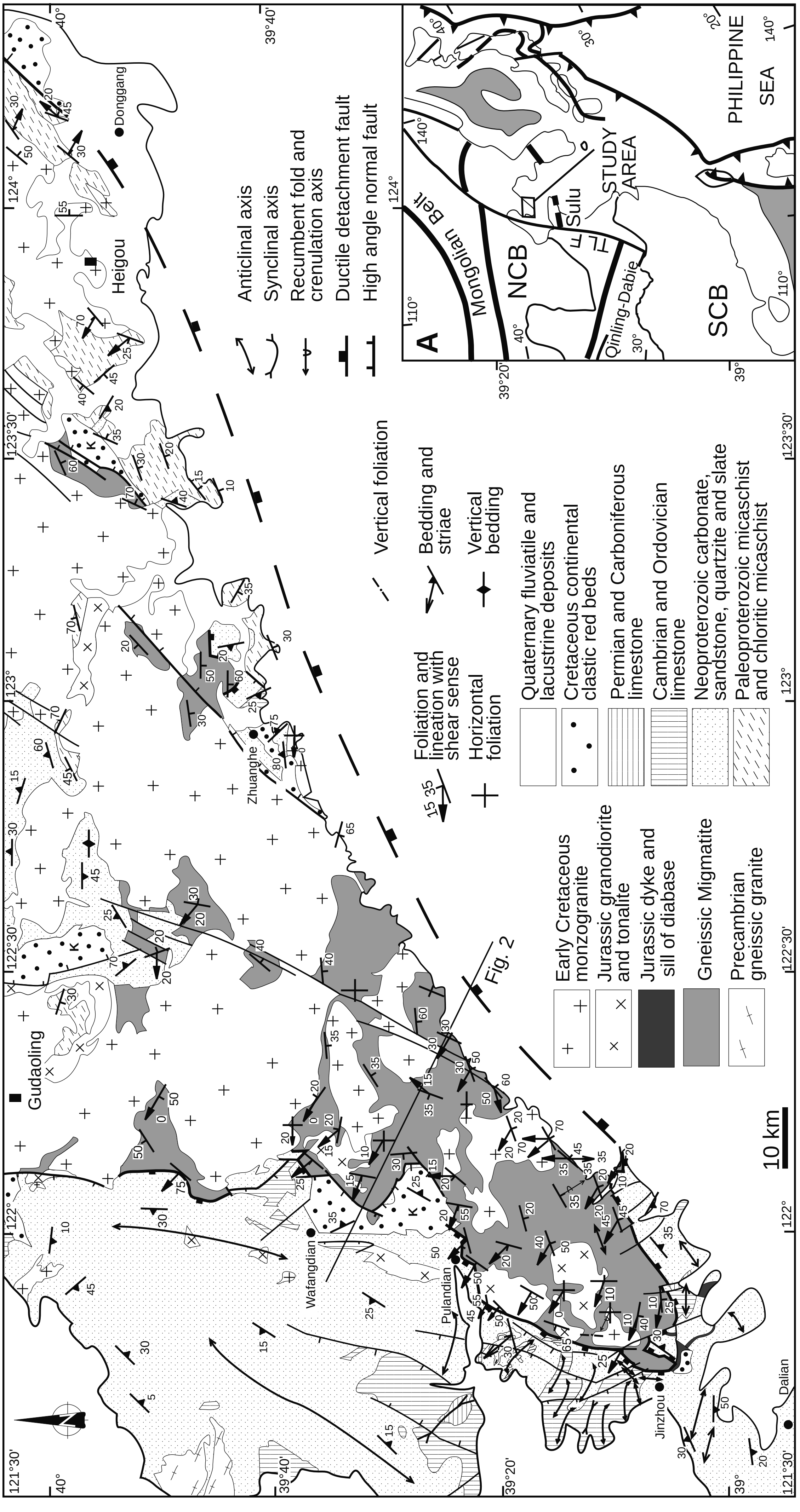

Gudaoling
Zhuanghe
Heigou
Donggang
Wafangdian
Pulandian
Jinzhou
Dalian
Fig. 2
10 km
121°30'
122°
122°30'
123°
123°30'
124°
40°
39°40'
39°20'
39°
A
NCB
SCB
Mongolian Belt
Qinling-Dabie
Sulu
STUDY AREA
PHILIPPINE SEA
Early Cretaceous monzogranite
Jurassic granodiorite and tonalite
Jurassic dyke and sill of diabase
Gneissic Migmatite
Precambrian gneissic granite
Quaternary fluviatile and lacustrine deposits
Cretaceous continental clastic red beds
Permian and Carboniferous limestone
Cambrian and Ordovician limestone
Neoproterozoic carbonate, sandstone, quartzite and slate
Paleoproterozoic micaschist and chloritic micaschist
Foliation and lineation with shear sense
Horizontal foliation
Vertical foliation
Bedding and striae
Vertical bedding
Anticlinal axis
Synclinal axis
Recumbent fold and crenulation axis
Ductile detachment fault
High angle normal fault
K

Figure 1

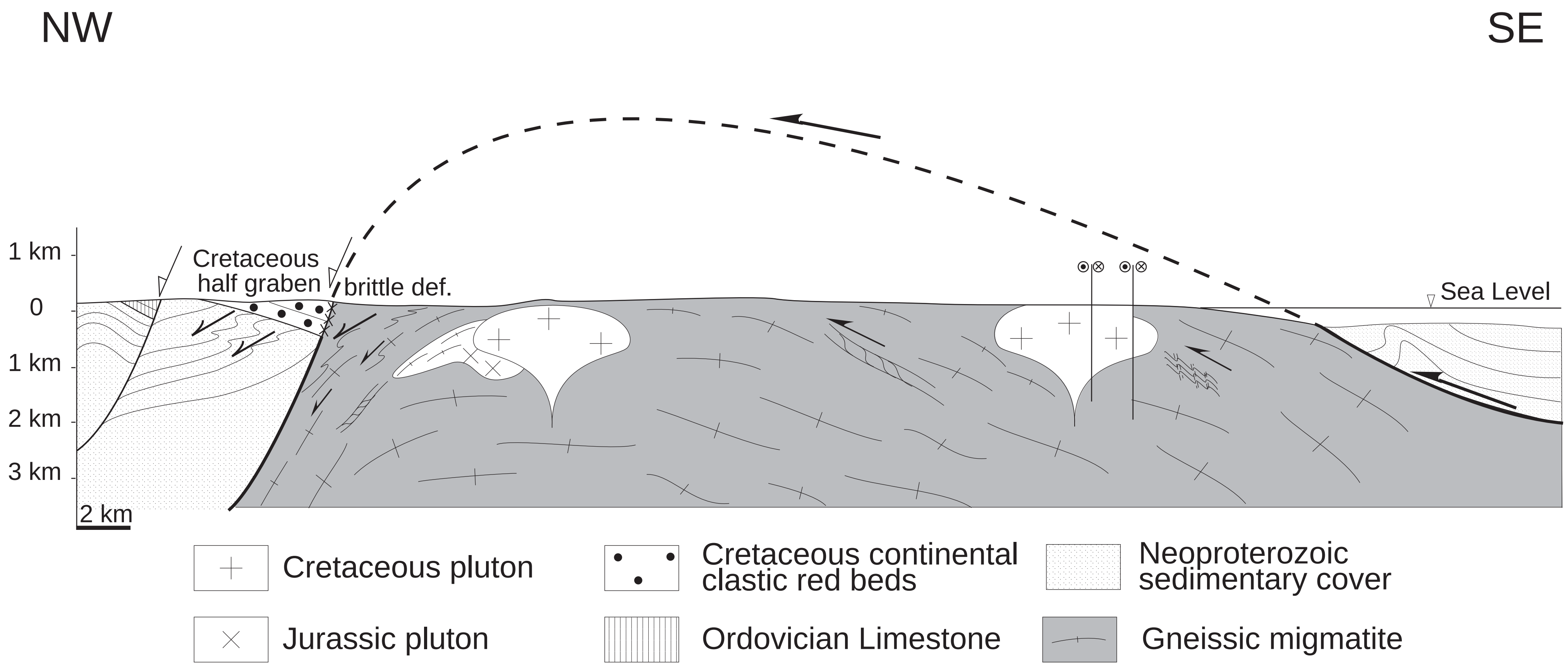
NW
SE
1 km
0
1 km
2 km
3 km
2 km
Cretaceous half graben
brittle def.
Sea Level
Cretaceous pluton
Jurassic pluton
Cretaceous continental clastic red beds
Ordovician Limestone
Neoproterozoic sedimentary cover
Gneissic migmatite

Figure 2

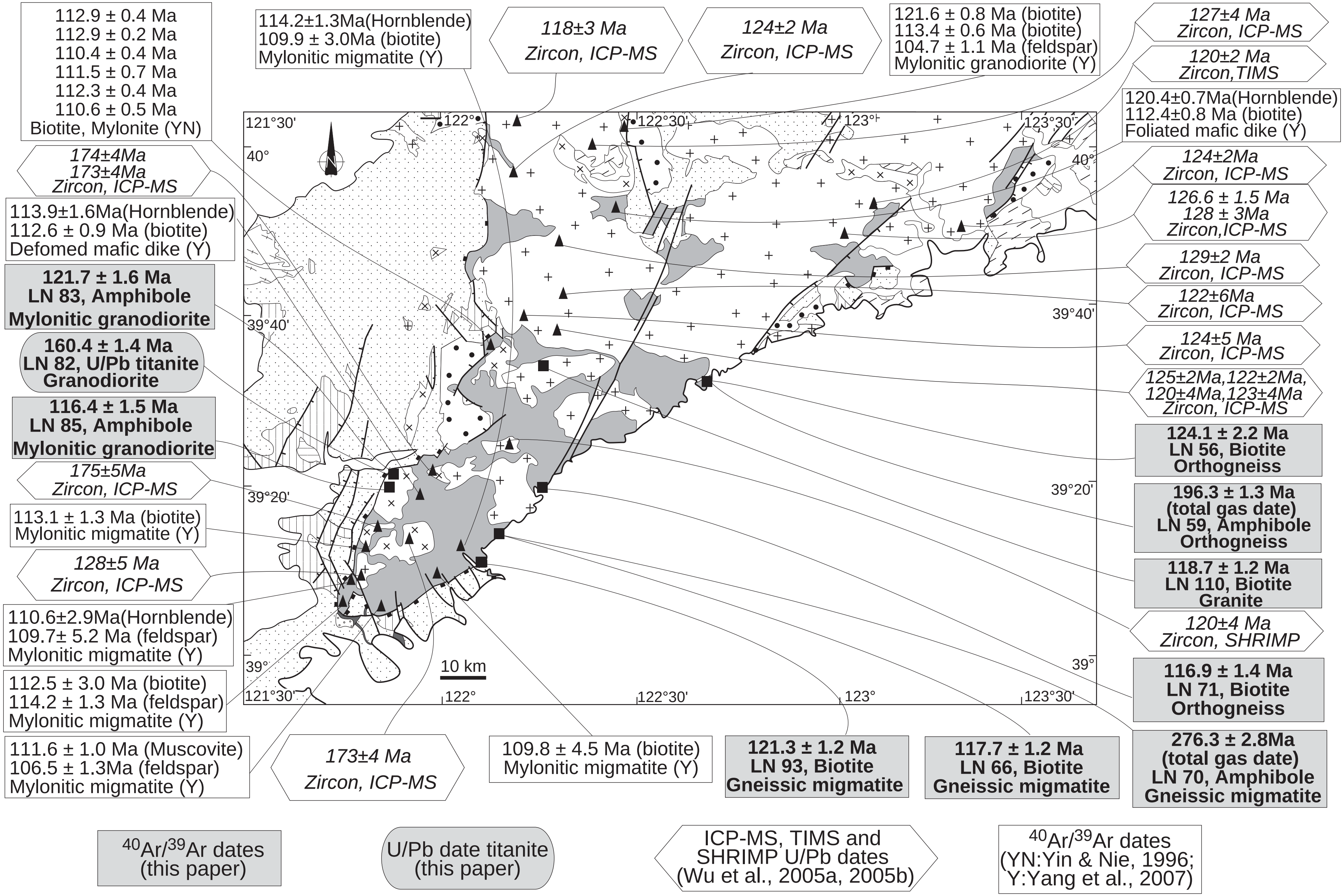
112.9 ± 0.4 Ma
112.9 ± 0.2 Ma
110.4 ± 0.4 Ma
111.5 ± 0.7 Ma
112.3 ± 0.4 Ma
110.6 ± 0.5 Ma
Biotite, Mylonite (YN)
114.2±1.3Ma(Hornblende)
109.9 ± 3.0Ma (biotite)
Mylonitic migmatite (Y)
118±3 Ma
Zircon, ICP-MS
124±2 Ma
Zircon, ICP-MS
121.6 ± 0.8 Ma (biotite)
113.4 ± 0.6 Ma (biotite)
104.7 ± 1.1 Ma (feldspar)
Mylonitic granodiorite (Y)
127±4 Ma
Zircon, ICP-MS
120±2 Ma
Zircon,TIMS
120.4±0.7Ma(Hornblende)
112.4±0.8 Ma (biotite)
Foliated mafic dike (Y)
174±4Ma
173±4Ma
Zircon, ICP-MS
113.9±1.6Ma(Hornblende)
112.6 ± 0.9 Ma (biotite)
Defomed mafic dike (Y)
121.7 ± 1.6 Ma
LN 83, Amphibole
Mylonitic granodiorite
160.4 ± 1.4 Ma
LN 82, U/Pb titanite
Granodiorite
116.4 ± 1.5 Ma
LN 85, Amphibole
Mylonitic granodiorite
175±5Ma
Zircon, ICP-MS
113.1 ± 1.3 Ma (biotite)
Mylonitic migmatite (Y)
128±5 Ma
Zircon, ICP-MS
110.6±2.9Ma(Hornblende)
109.7± 5.2 Ma (feldspar)
Mylonitic migmatite (Y)
112.5 ± 3.0 Ma (biotite)
114.2 ± 1.3 Ma (feldspar)
Mylonitic migmatite (Y)
111.6 ± 1.0 Ma (Muscovite)
106.5 ± 1.3Ma (feldspar)
Mylonitic migmatite (Y)
173±4 Ma
Zircon, ICP-MS
109.8 ± 4.5 Ma (biotite)
Mylonitic migmatite (Y)
121.3 ± 1.2 Ma
LN 93, Biotite
Gneissic migmatite
117.7 ± 1.2 Ma
LN 66, Biotite
Gneissic migmatite
276.3 ± 2.8Ma
(total gas date)
LN 70, Amphibole
Gneissic migmatite
124±2Ma
Zircon, ICP-MS
126.6 ± 1.5 Ma
128 ± 3Ma
Zircon,ICP-MS
129±2 Ma
Zircon, ICP-MS
122±6Ma
Zircon, ICP-MS
124±5 Ma
Zircon, ICP-MS
125±2Ma,122±2Ma,
120±4Ma,123±4Ma
Zircon, ICP-MS
124.1 ± 2.2 Ma
LN 56, Biotite
Orthogneiss
196.3 ± 1.3 Ma
(total gas date)
LN 59, Amphibole
Orthogneiss
118.7 ± 1.2 Ma
LN 110, Biotite
Granite
120±4 Ma
Zircon, SHRIMP
116.9 ± 1.4 Ma
LN 71, Biotite
Orthogneiss
121°30'
122°
122°30'
123°
123°30'
40°
39°40'
39°20'
39°
10 km
⁴⁰Ar/³⁹Ar dates
(this paper)
U/Pb date titanite
(this paper)
ICP-MS, TIMS and
SHRIMP U/Pb dates
(Wu et al., 2005a, 2005b)
⁴⁰Ar/³⁹Ar dates
(YN:Yin & Nie, 1996;
Y:Yang et al., 2007)

Figure 3

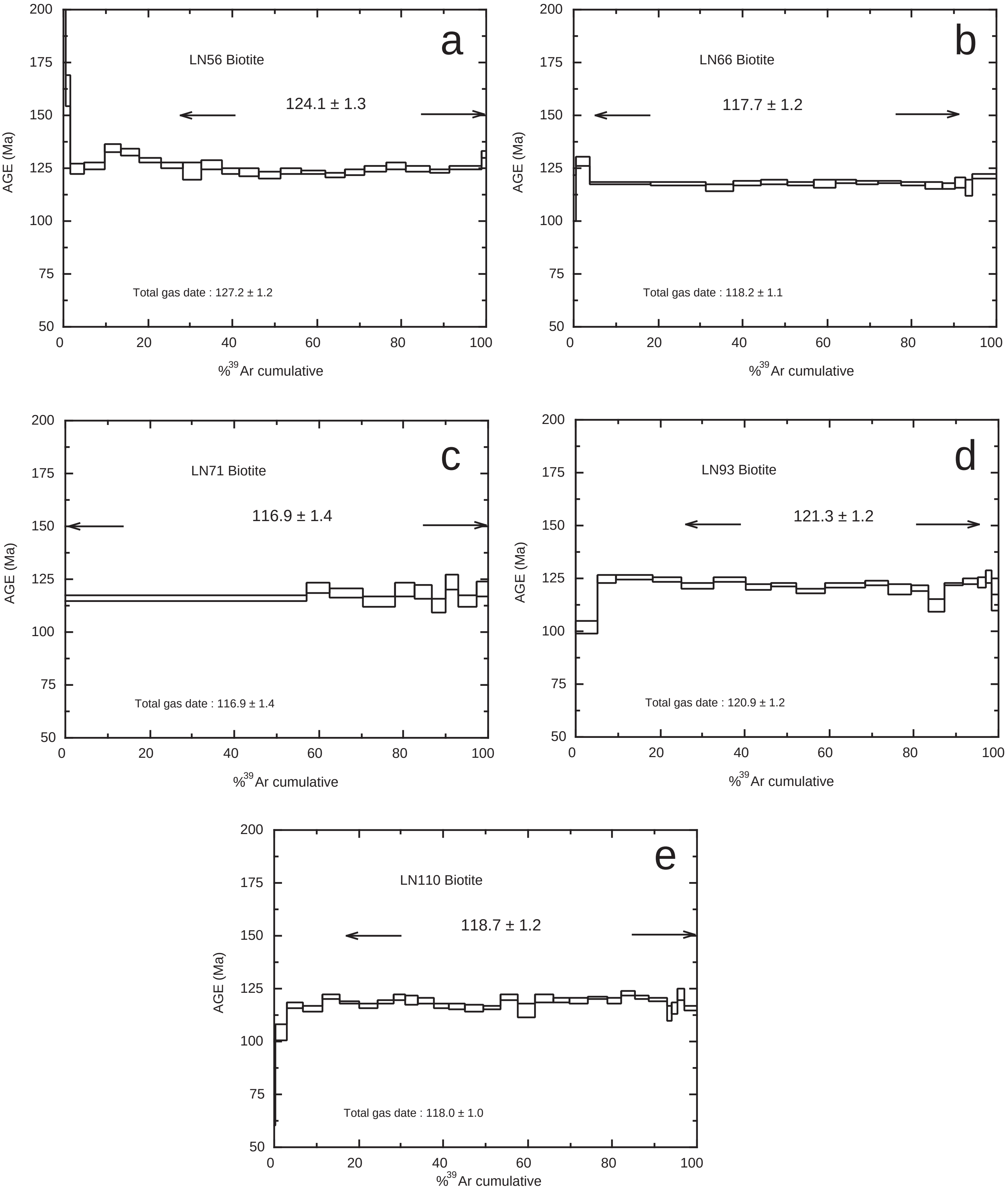
a
LN56 Biotite
124.1 ± 1.3
Total gas date : 127.2 ± 1.2
b
LN66 Biotite
117.7 ± 1.2
Total gas date : 118.2 ± 1.1
c
LN71 Biotite
116.9 ± 1.4
Total gas date : 116.9 ± 1.4
d
LN93 Biotite
121.3 ± 1.2
Total gas date : 120.9 ± 1.2
e
LN110 Biotite
118.7 ± 1.2
Total gas date : 118.0 ± 1.0
AGE (Ma)
200
175
150
125
100
75
50
0
20
40
60
80
100
%39Ar cumulative

Figure 4

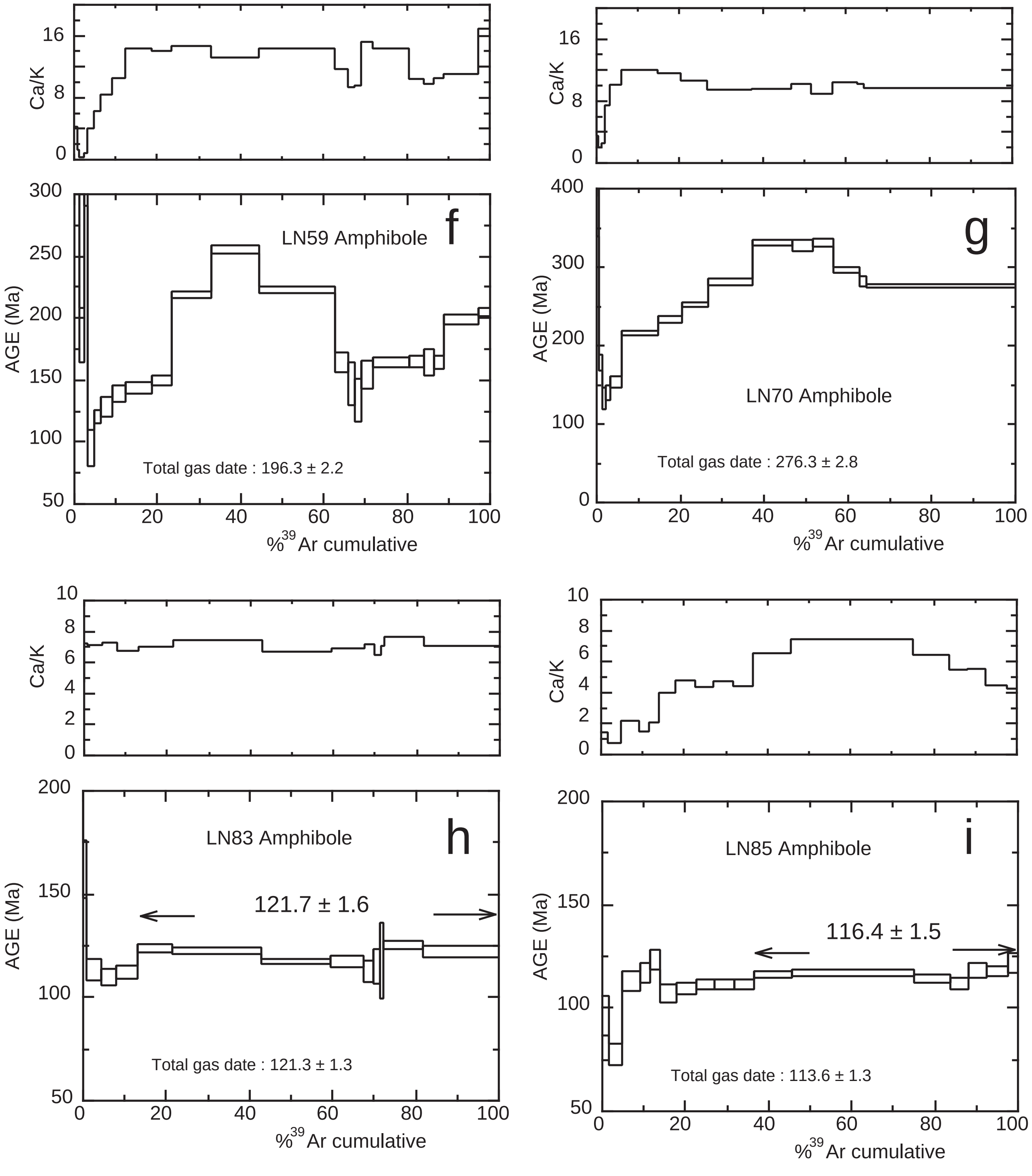
Ca/K
16
8
0
300
250
200
150
100
50
AGE (Ma)
f
LN59 Amphibole
Total gas date : 196.3 ± 2.2
0
20
40
60
80
100
%^{39}Ar cumulative
Ca/K
16
8
0
400
300
200
100
0
AGE (Ma)
g
LN70 Amphibole
Total gas date : 276.3 ± 2.8
0
20
40
60
80
100
%^{39}Ar cumulative
Ca/K
10
8
6
4
2
0
200
150
100
50
AGE (Ma)
h
LN83 Amphibole
121.7 ± 1.6
Total gas date : 121.3 ± 1.3
0
20
40
60
80
100
%^{39}Ar cumulative
Ca/K
10
8
6
4
2
0
200
150
100
50
AGE (Ma)
i
LN85 Amphibole
116.4 ± 1.5
Total gas date : 113.6 ± 1.3
0
20
40
60
80
100
%^{39}Ar cumulative

Figure 4

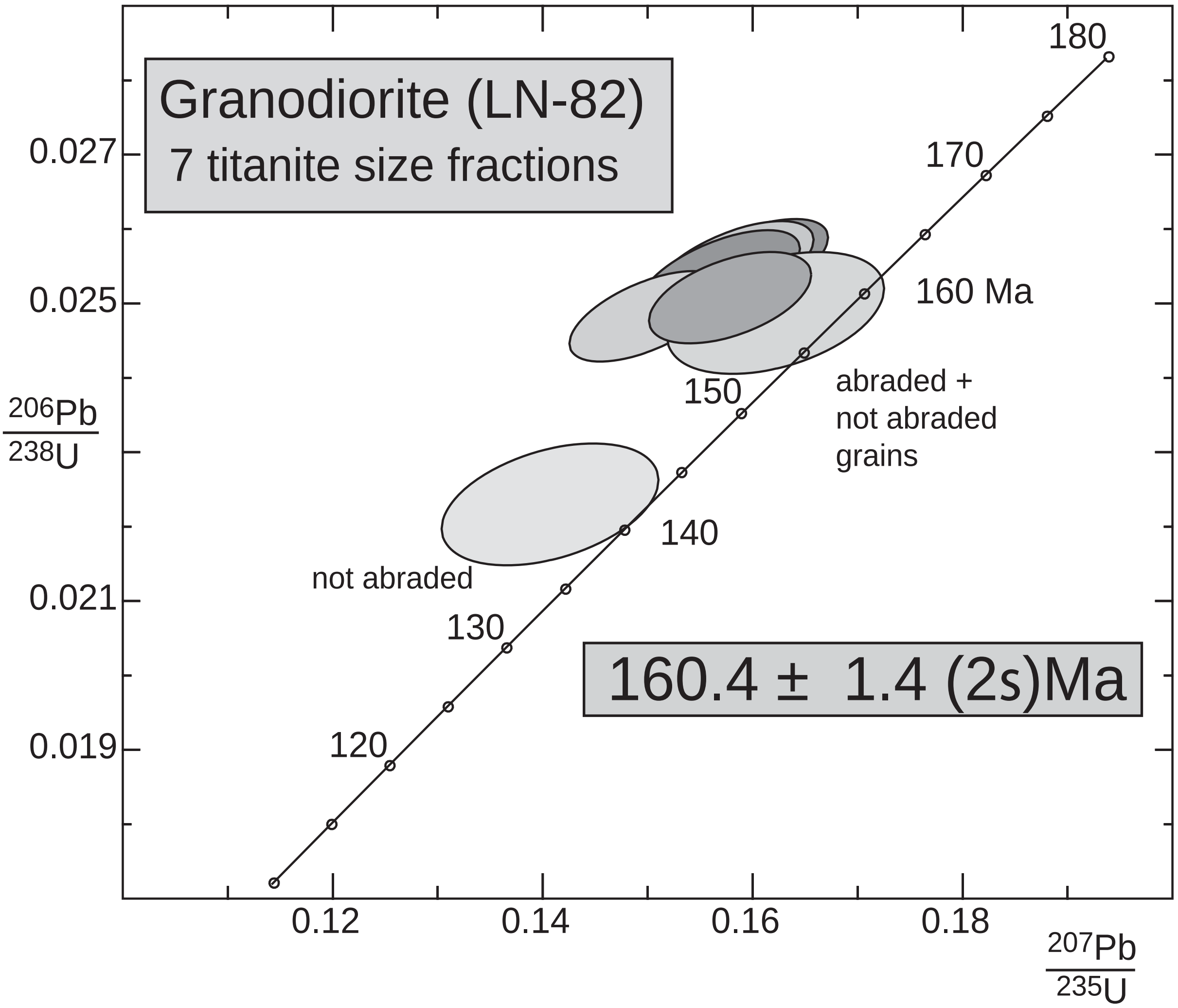
Granodiorite (LN-82)
7 titanite size fractions
160.4 ± 1.4 (2s)Ma
180
170
160 Ma
150
140
130
120
abraded +
not abraded
grains
not abraded
0.027
0.025
0.021
0.019
0.12
0.14
0.16
0.18
206Pb/238U
207Pb/235U

Figure 5

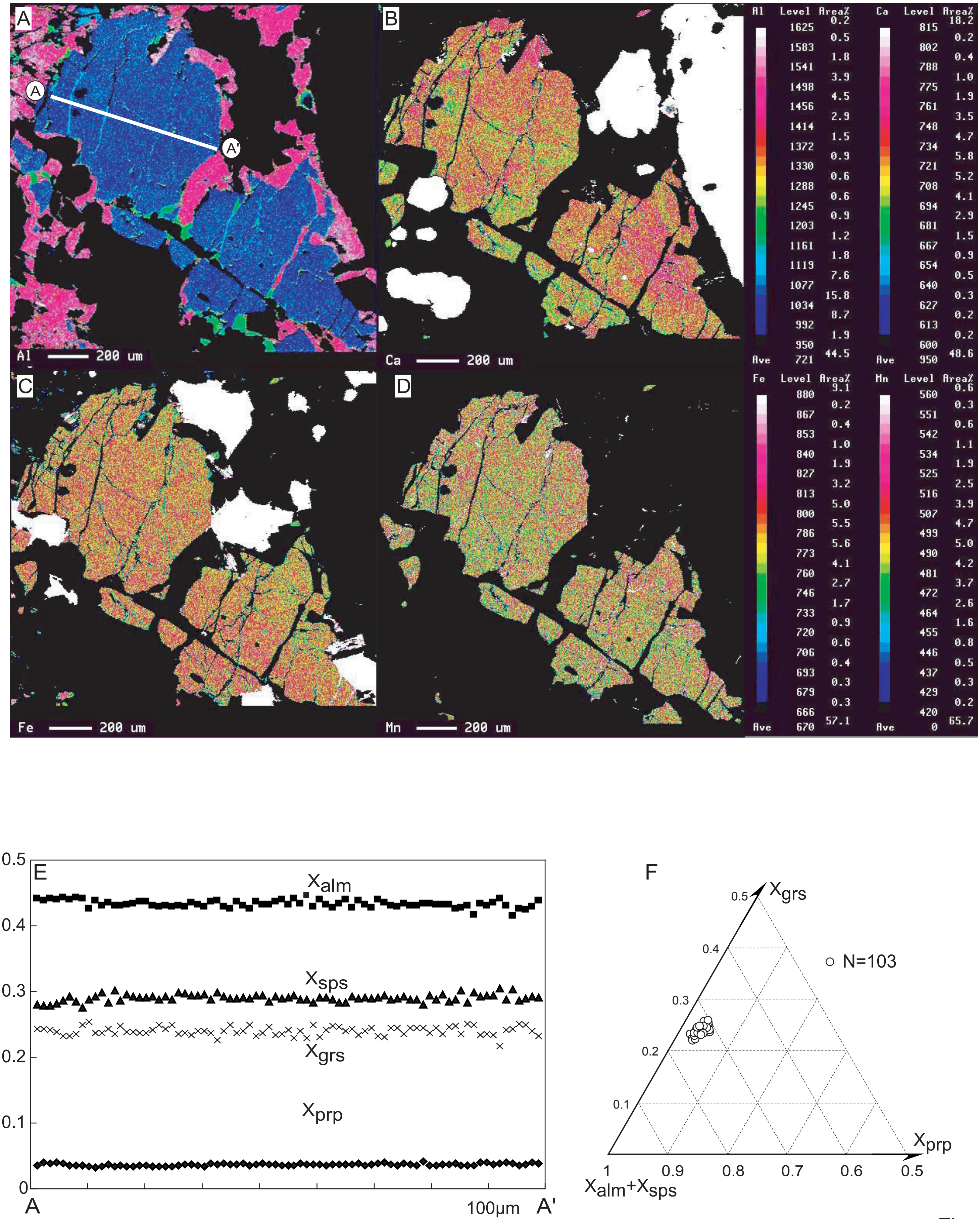
A
A
A'
Al 200 um
B
Ca 200 um
C
Fe 200 um
D
Mn 200 um
Al Level Area%
Ca Level Area%
Fe Level Area%
Mn Level Area%
Ave
E
Xalm
Xsps
Xgrs
Xprp
0.5
0.4
0.3
0.2
0.1
0
A
100µm
A'
F
Xgrs
0.5
0.4
0.3
0.2
0.1
○ N=103
Xprp
1
0.9
0.8
0.7
0.6
0.5
Xalm+Xsps

Fig. 6

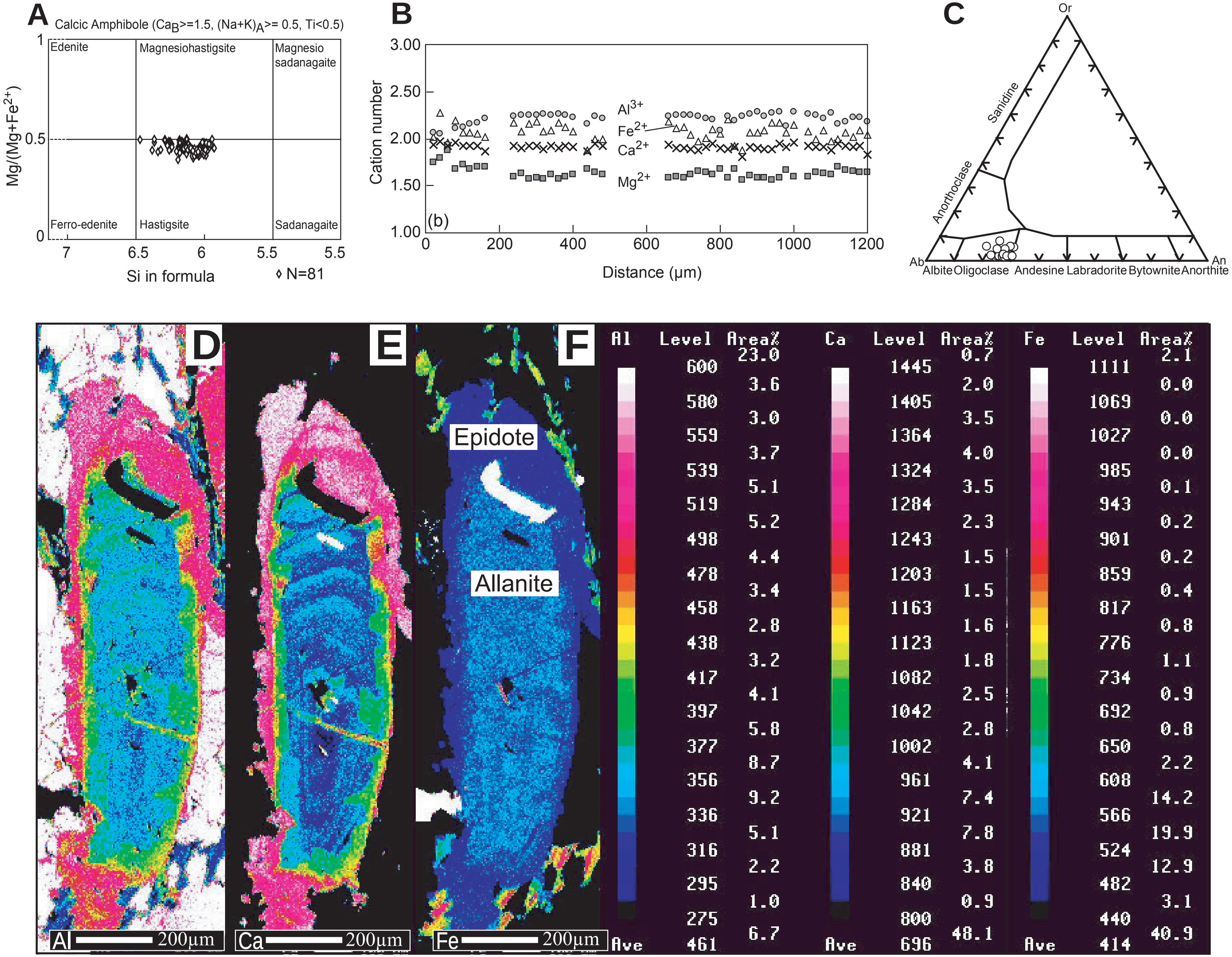
A
Calcic Amphibole (Ca_B>=1.5, $(Na+K)_A$>= 0.5, Ti<0.5)
Edenite
Magnesiohastigsite
Magnesio sadanagaite
Ferro-edenite
Hastigsite
Sadanagaite
Mg/(Mg+Fe^{2+})
1
0.5
0
7
6.5
6
5.5
5.5
Si in formula
◊ N=81
B
Cation number
3.00
2.50
2.00
1.50
1.00
(b)
Al^{3+}
Fe^{2+}
Ca^{2+}
Mg^{2+}
0
200
400
600
800
1000
1200
Distance (μm)
C
Or
Sanidine
Anorthoclase
Ab
An
Albite
Oligoclase
Andesine
Labradorite
Bytownite
Anorthite
D
E
F
Epidote
Allanite
Al 200μm
Ca 200μm
Fe 200μm
Al Level Area%
600 23.0
580 3.6
559 3.0
539 3.7
519 5.1
498 5.2
478 4.4
458 3.4
438 2.8
417 3.2
397 4.1
377 5.8
356 8.7
336 9.2
316 5.1
295 2.2
275 1.0
Ave 461 6.7
Ca Level Area%
1445 0.7
1405 2.0
1364 3.5
1324 4.0
1284 3.5
1243 2.3
1203 1.5
1163 1.5
1123 1.6
1082 1.8
1042 2.5
1002 2.8
961 4.1
921 7.4
881 7.8
840 3.8
800 0.9
Ave 696 48.1
Fe Level Area%
1111 2.1
1069 0.0
1027 0.0
985 0.0
943 0.1
901 0.2
859 0.2
817 0.4
776 0.8
734 1.1
692 0.9
650 0.8
608 2.2
566 14.2
524 19.9
482 12.9
440 3.1
Ave 414 40.9

Fig. 7

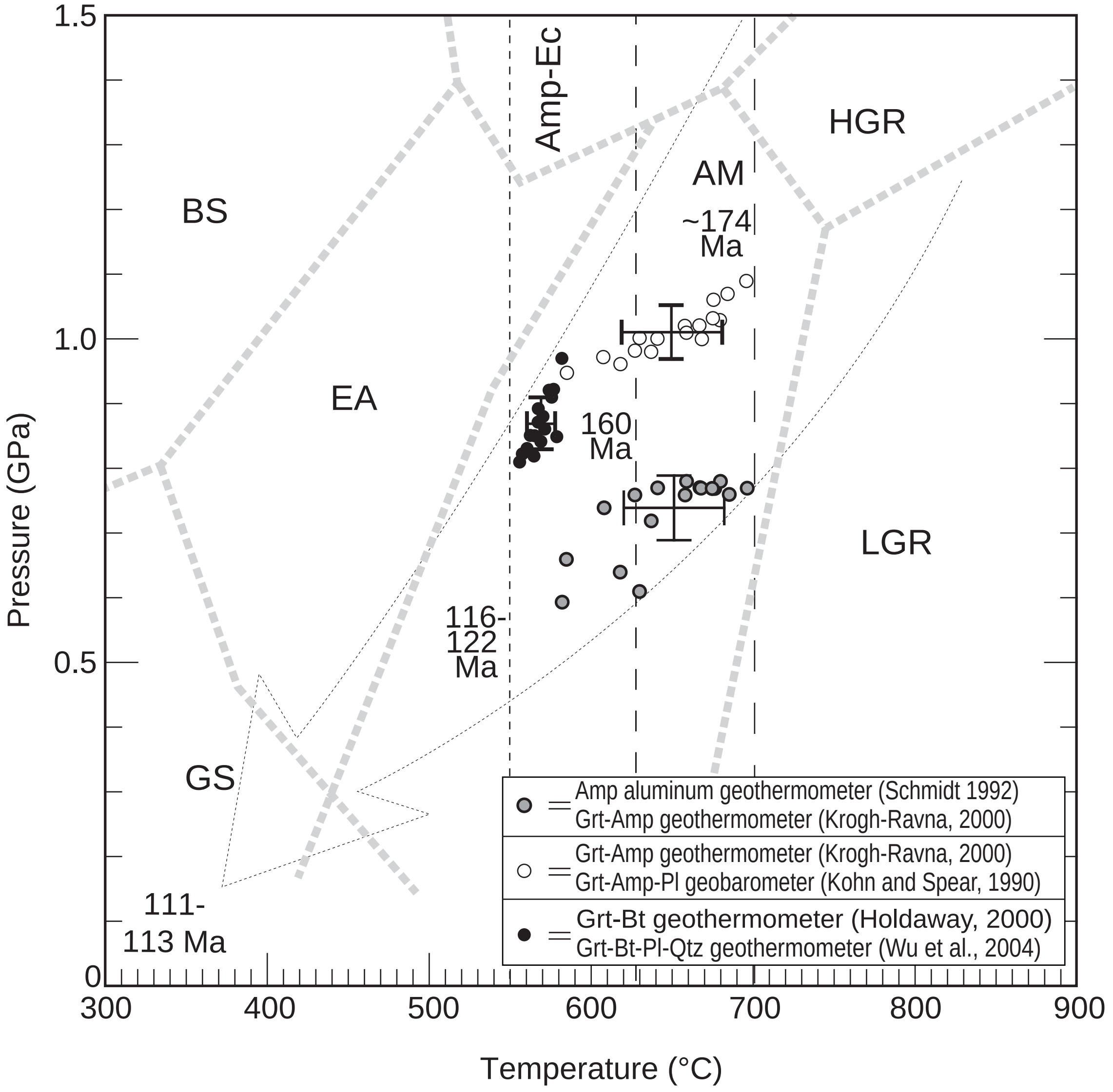

Pressure (GPa)
1.5
1.0
0.5
0
Temperature (°C)
300
400
500
600
700
800
900
Amp-Ec
BS
EA
GS
AM
HGR
LGR
~174 Ma
160 Ma
116-122 Ma
111-113 Ma
● = Amp aluminum geothermometer (Schmidt 1992) Grt-Amp geothermometer (Krogh-Ravna, 2000)
○ = Grt-Amp geothermometer (Krogh-Ravna, 2000) Grt-Amp-Pl geobarometer (Kohn and Spear, 1990)
● = Grt-Bt geothermometer (Holdaway, 2000) Grt-Bt-Pl-Qtz geothermometer (Wu et al., 2004)

Fig. 8

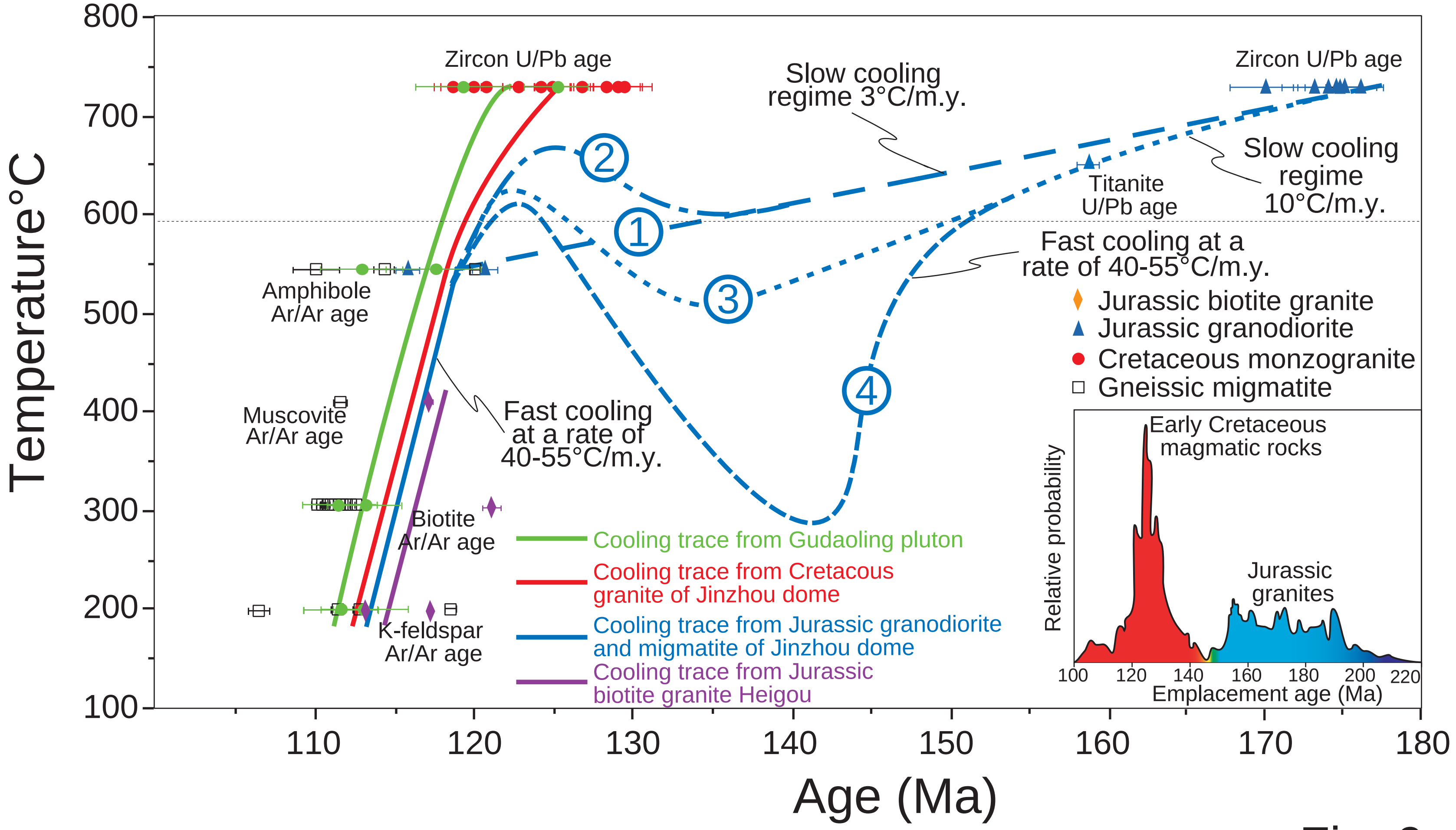
Temperature°C
800
700
600
500
400
300
200
100
Age (Ma)
110
120
130
140
150
160
170
180
Zircon U/Pb age
Zircon U/Pb age
Slow cooling regime 3°C/m.y.
Slow cooling regime 10°C/m.y.
Titanite U/Pb age
Fast cooling at a rate of 40-55°C/m.y.
Fast cooling at a rate of 40-55°C/m.y.
①
②
③
④
Amphibole Ar/Ar age
Muscovite Ar/Ar age
Biotite Ar/Ar age
K-feldspar Ar/Ar age
Cooling trace from Gudaoling pluton
Cooling trace from Cretacous granite of Jinzhou dome
Cooling trace from Jurassic granodiorite and migmatite of Jinzhou dome
Cooling trace from Jurassic biotite granite Heigou
♦ Jurassic biotite granite
▲ Jurassic granodiorite
● Cretaceous monzogranite
□ Gneissic migmatite
Relative probability
Early Cretaceous magmatic rocks
Jurassic granites
100
120
140
160
180
200
220
Emplacement age (Ma)

Fig. 9

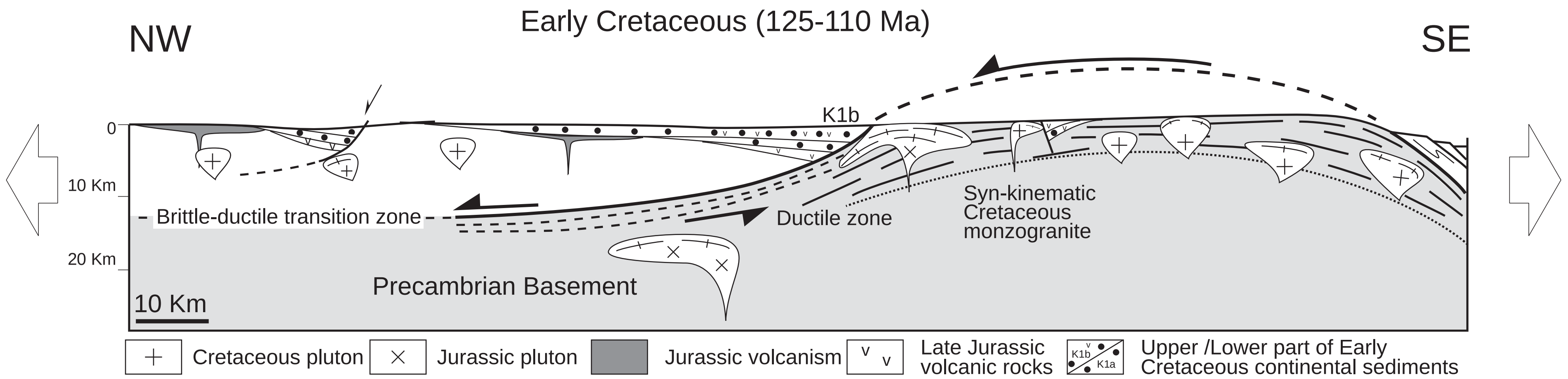
Early Cretaceous (125-110 Ma)
NW
SE
0
10 Km
20 Km
K1b
Brittle-ductile transition zone
Ductile zone
Syn-kinematic
Cretaceous
monzogranite
Precambrian Basement
10 Km
Cretaceous pluton
Jurassic pluton
Jurassic volcanism
Late Jurassic
volcanic rocks
K1b
K1a
Upper /Lower part of Early
Cretaceous continental sediments

Fig. 10